ANNUAL REVIEWS

Annual Review of Astronomy and Astrophysics

Astrochemistry During the Formation of Stars

Jes K. Jørgensen,[1] Arnaud Belloche,[2] and Robin T. Garrod[3]

[1]Niels Bohr Institute, University of Copenhagen, 1350 Copenhagen, Denmark; email: jeskj@nbi.ku.dk

[2]Max-Planck-Institut für Radioastronomie, 53121 Bonn, Germany; email: belloche@mpifr-bonn.mpg.de

[3]Departments of Chemistry and Astronomy, University of Virginia, Charlottesville, Virginia 22904, USA; email: rgarrod@virginia.edu

Annu. Rev. Astron. Astrophys. 2020. 58:727–78

First published as a Review in Advance on July 24, 2020

The *Annual Review of Astronomy and Astrophysics* is online at astro.annualreviews.org

https://doi.org/10.1146/annurev-astro-032620-021927

Keywords

complex molecules, interstellar medium, interstellar molecules, star formation, submillimeter astronomy

Abstract

Star-forming regions show a rich and varied chemistry, including the presence of complex organic molecules—in both the cold gas distributed on large scales and the hot regions close to young stars where protoplanetary disks arise. Recent advances in observational techniques have opened new possibilities for studying this chemistry. In particular, the Atacama Large Millimeter/submillimeter Array has made it possible to study astrochemistry down to Solar System–size scales while also revealing molecules of increasing variety and complexity. In this review, we discuss recent observations of the chemistry of star-forming environments, with a particular focus on complex organic molecules, taking context from the laboratory experiments and chemical models that they have stimulated. The key takeaway points include the following:

- The physical evolution of individual sources plays a crucial role in their inferred chemical signatures and remains an important area for observations and models to elucidate.
- Comparisons of the abundances measured toward different star-forming environments (high-mass versus low-mass, Galactic Center versus Galactic disk) reveal a remarkable similarity, which is an indication that the underlying chemistry is relatively independent of variations in their physical conditions.

- Studies of molecular isotopologues in star-forming regions provide a link with measurements in our own Solar System, and thus may shed light on the chemical similarities and differences expected in other planetary systems.

Contents

1. INTRODUCTION

1.1. Motivation

The environments in which young stars form show a rich and varied chemistry. In fact, most of the molecules detected in the interstellar medium (ISM) to date have first been found in these regions—whether in the cold starless/prestellar cores or in the warm gas surrounding young stars of high or low masses. These species range all the way from simple diatomic and triatomic neutral molecules to molecular radicals and ions, to complex molecules. The latter, some with ten atoms or more, include species containing long unsaturated chains of carbon atoms as well as saturated organics that can be considered the starting points for eventual prebiotic chemistry. The chemical networks describing the formation and destruction paths for these different species are strongly dependent on the underlying physical evolution of the star-formation processes, such as the changes in density, temperature, and spectral shape and intensity of irradiation.

Although molecules of varying degrees of complexity have also been detected in other regions including the envelopes around evolved stars, photodissociation regions, well-developed protoplanetary disks around Class II young stellar objects (YSOs)/T Tauri stars, and even distant galaxies, the chemistry in prestellar cores of molecular clouds and embedded protostellar stages is critical. These stages provide key laboratories for molecular astrophysics: Thanks to the characteristically high molecular column densities of these sources, they have yielded by far the most complete chemical inventories of any interstellar object, including censuses of low-abundance organics and their isotopologues. Also, these stages are likely pivotal for linking the birth environments of young stars and the initial conditions in the emerging protoplanetary disks in terms of both their physics and chemistry.

However, these sources also illustrate some of the major challenges in terms of understanding astrochemistry. In particular, recent observations with significant improvements in sensitivity and spatial resolution have revealed that complex chemistry is taking place in a wider range of the physical components of young protostars than considered previously (**Figure 1**). Understanding how the physical structure and evolution of young protostars influences the degree of molecular complexity that arises in their envelopes and disks, and how this may further influence chemical composition during the later planet-forming stages, remain some of the key challenges for astrochemistry.

1.2. Star Formation and Astrochemistry

The canonical scenario for the formation of a solar-type protostar starts at low temperatures of $\sim$10 K at densities of 10^3–10^4 cm^{-3} with the formation of a dense prestellar core in a giant molecular cloud. In the denser parts of such cores, gaseous molecules collide with and stick to the surfaces of dust grains during their earliest stages and cold gas-phase chemistry leads to abundance enhancements of, e.g., deuterium-containing molecules through fractionation. Star formation occurs when these cores collapse, leading to the formation of an opaque (second) hydrostatic core. Further infall leads to the release of gravitational potential energy heating the infalling envelope of dust and gas to temperatures of tens or hundreds of kelvins, whereas the densities increase to $\sim 10^8$–10^9 cm^{-3} in the inner $\sim$100-au (astronomical unit) regions around the central protostar. As the temperatures increase above 100 K, the water-rich ice mantles sublimate, injecting molecules into the gas phase, giving rise to the so-called hot corino regions at high temperatures and densities, which are rich in saturated complex organics. These are also the scales at which protoplanetary disks are expected to arise owing to the conservation of angular momentum, a process that also leads to the launching of outflows and jets. Although the overall physical evolution for high-mass

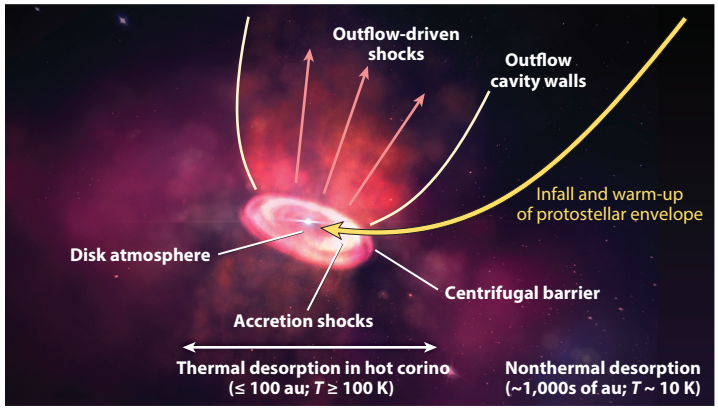

Figure 1

Schematic representation of a young solar-type protostar and its structural components that are key to its chemistry. Complex organic molecules are observed to be present in all of these components as the result of thermal and nonthermal desorption: on small and large scales within the protostellar envelope and disk, in shocks related to accretion at the disk surface and centrifugal barrier, and on larger scales associated with the protostellar outflow. UV irradiation close to the disk and outflow cavity are also potentially important in regulating the chemistry. The main focus of the previous review in this series by Herbst & van Dishoeck (2009) was on the formation of complex organic species during the infall/warm-up phase (*thick yellow arrow*; see Herbst & van Dishoeck 2009, their figure 14), but, as discussed in this review, in recent years a much more complex picture has emerged. Background image by Per Bjerkeli. Abbreviation: au, astronomical unit.

stars through these stages is clearly more complex, many of the overall characteristics can be identified, including the extended hot cores with elevated temperatures, within which complex organics are present in some cases. Due to the high column densities of warm material, many of the first detections of complex organic molecules (COMs)[1] were made toward these high-mass regions.

The topic of astrochemistry and its link to star formation has been the subject of previous reviews in this journal.[2] Van Dishoeck & Blake (1998) focused on the overall chemical evolution of star-forming regions that at the time had come within reach through advances in (sub)millimeter wavelength single-dish telescopes, space-borne IR telescopes, and previous generations of millimeter-wavelength interferometers. These efforts underlined the importance of molecular astrophysics as a tracer of the physical changes taking place during the star-formation process. This includes the freeze-out of molecules on the surfaces of dust grains, the resulting grain-surface chemistry leading to more complex species, and eventually the release of those

[1] We keep the definition proposed by Herbst & van Dishoeck (2009) and widely used in the community: a COM is a carbon-bearing molecule that has at least six atoms. Alternative names such as large astronomical molecule (LAM) or interstellar complex organic molecule (iCOM) have been proposed in the past decade, but as long as the context (astrochemistry, not biology or chemistry) is clear and the definition is stated, the term COM is adequate.

[2] In addition to the mentioned reviews from this journal, it is worth pointing out a number of reviews from the past decade: Tielens (2013) described the physical and chemical processes governing the formation and evolution of molecules in the ISM; Caselli & Ceccarelli (2012) and Ceccarelli et al. (2014) addressed the link between astrochemistry in star-forming regions and the Solar System; Boogert et al. (2015) discussed observations of ices; and van Dishoeck et al. (2014) investigated the water trail through the star-formation process. A review on recent developments in millimeter/submillimeter laboratory spectroscopy in support of observational astrochemistry was presented by Widicus Weaver (2019).

molecules into the gas phase during the collapse due to thermal desorption close to young stars or in outflow-driven shocks or their incorporation into protoplanetary disks.

A decade later, dedicated observational efforts, laboratory studies, and sophisticated gas-phase and grain-surface chemical models had shifted the focus from the relatively simple species to the formation of COMs, which was the subject of the review by Herbst & van Dishoeck (2009). Extensive observations of hot cores had provided the first unbiased surveys providing complete censuses of the molecular line content of individual high-mass protostars covering wide spectral ranges of the windows where the atmosphere is mostly transparent, as well as systematic, more focused, inventories of networks of species toward groups of sources. Targeted observations of low-mass protostars had started revealing the rich chemistries of these sources as well, including the detections of saturated complex organics in the inner envelopes of deeply embedded protostars as well as in shocks associated with their outflows.

Today, yet another decade later, gigantic steps forward have been taken due to the systematic molecular studies at terahertz frequencies by the *Herschel Space Observatory* (*Herschel*); significant upgrades to many (sub)millimeter wavelength single-dish telescopes and interferometers especially in terms of the receivers and correlators; and, in particular, the advent of the Atacama Large Millimeter/submillimeter Array (ALMA) that has pushed molecular astrophysics studies by orders of magnitude in sensitivity and spatial resolution.

1.3. Outline of This Review

In this review, we focus on the complex chemistry taking place from the point at which star formation is initiated by the formation of dense (prestellar) cores, through their collapse to form young protostars and their circumstellar disks. We describe the opportunities and challenges encountered with recent advances in observations, modeling, and laboratory experiments (Section 2) and provide an overview of detections of complex molecules in different environments (Section 3). This is followed by discussions of the importance of the physical conditions on the chemistry reflecting both the nonhomogeneous conditions in star-forming environments (Section 4) and the changes occurring during the formation and early evolution of stars (Section 5). The final two sections focus on constraints on the formation of complex organic molecules and the link between star-forming environments and our own Solar System. Specifically, we describe the insights that can be obtained by studies of isotopic fractionation (Section 6) and by comparing systematic chemical inventories across samples of sources to measurements from our own Solar System and the predictions from models (Section 7).

2. RECENT ADVANCES AND NEW CHALLENGES

2.1. Advances in Observational Techniques

Significant advances within astrochemistry have been made over the past decade thanks to new telescopes (see the sidebar titled New Facilities) and improvements in instrumentation at existing facilities. The key features offered by these facilities are (*a*) the improvement in the large instantaneous bandwidths covered with high spectral resolution by individual instruments, (*b*) the sensitivity offered by large apertures and excellent observation sites, (*c*) improved spatial resolution with, in particular, combined array antennas, and (*d*) coverage of high-frequency windows in the far-IR with high spectral resolution using space-based telescopes such as *Herschel* and the SOFIA (Stratospheric Observatory for Infrared Astronomy). Each of these aspects provides new opportunities as well as challenges.

NEW FACILITIES

The three main new facilities for studies of star-forming regions that have started operations in the past decade are:

- **Atacama Large Millimeter/submillimeter Array (ALMA):** 66-telescope array operating at submillimeter wavelengths. ALMA has demonstrated its métier for high-resolution, high-sensitivity imaging of the distribution of molecules in star-forming regions both near and far (2011–).
- ***Herschel Space Observatory*** **(*Herschel*):** 3.5-m space-based observatory operating at far-IR (THz) wavelengths. Key contributions concern the presence of water and organics in star-forming regions (2009–2013).
- **Stratospheric Observatory for Infrared Astronomy (SOFIA):** 2.5-m airborne telescope that gives access to far-IR windows not observable from the ground, particularly to important cooling lines of the ISM (2010–).

2.1.1. Increase of instantaneous bandwidth at many observational facilities. One of the key aspects of *Herschel* and ALMA, as well as upgrades of receivers and correlators on facilities such as the APEX (Atacama Pathfinder EXperiment), the Institut de Radioastronomie Millimétrique (IRAM) 30-m telescope, the NOrthern Extended Millimeter Array (NOEMA), and the Submillimeter Array (SMA), has been the increase in instantaneous bandwidth obtainable while keeping a relatively high spectral resolution. This is particularly important for performing unbiased spectral surveys covering large frequency ranges. For example, the HEXOS (Herschel observations of EXtra-Ordinary Sources) survey of Orion performed a spectral scan from 480 to 1907 GHz (with two small gaps) with 1.1-MHz spectral resolution and identified more than 13,000 spectral lines, i.e., 10 lines per gigahertz (Crockett et al. 2014). From ALMA the Exploring Molecular Complexity with ALMA (EMoCA) survey of the high-mass star-forming region Sgr B2(N) (Belloche et al. 2016) and the Protostellar Interferometric Line Survey (PILS) of the nearby low-mass protostar IRAS 16293-2422 (Jørgensen et al. 2016) have been the main unbiased studies. The high angular resolution of EMoCA revealed that the secondary hot core Sgr B2(N2), with about 6,500 lines detected above 7σ between 84 and 114 GHz (about 220 lines per gigahertz), has narrow lines ($\sim$5 km s^{-1}) compared to the lines measured with single-dish telescopes toward Sgr B2(N). This reduction in spectral confusion was decisive for the identification of new species. The main component of PILS was a systematic survey of the 329–363-GHz range of ALMA's Band 7 at 0.25 km s^{-1} spectral resolution (see **Figure 2**). With the narrow lines ($\sim$1 km s^{-1}) at selected positions toward the protostellar system, the line confusion is reached at low levels, and more than 10,000 lines above 5σ can be identified (about 300 lines per gigahertz).

The key advantage of large bandwidth lies in the possibility for identifications of new species as well as accurate modeling of line emission leading to robust derivations of excitation temperatures and column densities. In particular, secure identifications of new species need a high number of well-isolated lines that can be assigned and modeled (see Section 2.2). Furthermore, with access to larger bandwidths, the range of energy levels and line strengths covered by individual species provides highly accurate constraints on their excitation. With of order 15–20 identified lines, the typical uncertainties on excitation temperatures and column densities become less than 10–20% when local thermodynamic equilibrium (LTE) can be assumed (e.g., Jørgensen et al. 2018). Laboratory astrophysics has also benefited from these technical developments (see Widicus Weaver 2019, and references therein). New spectrometers with large bandwidths are starting to be used

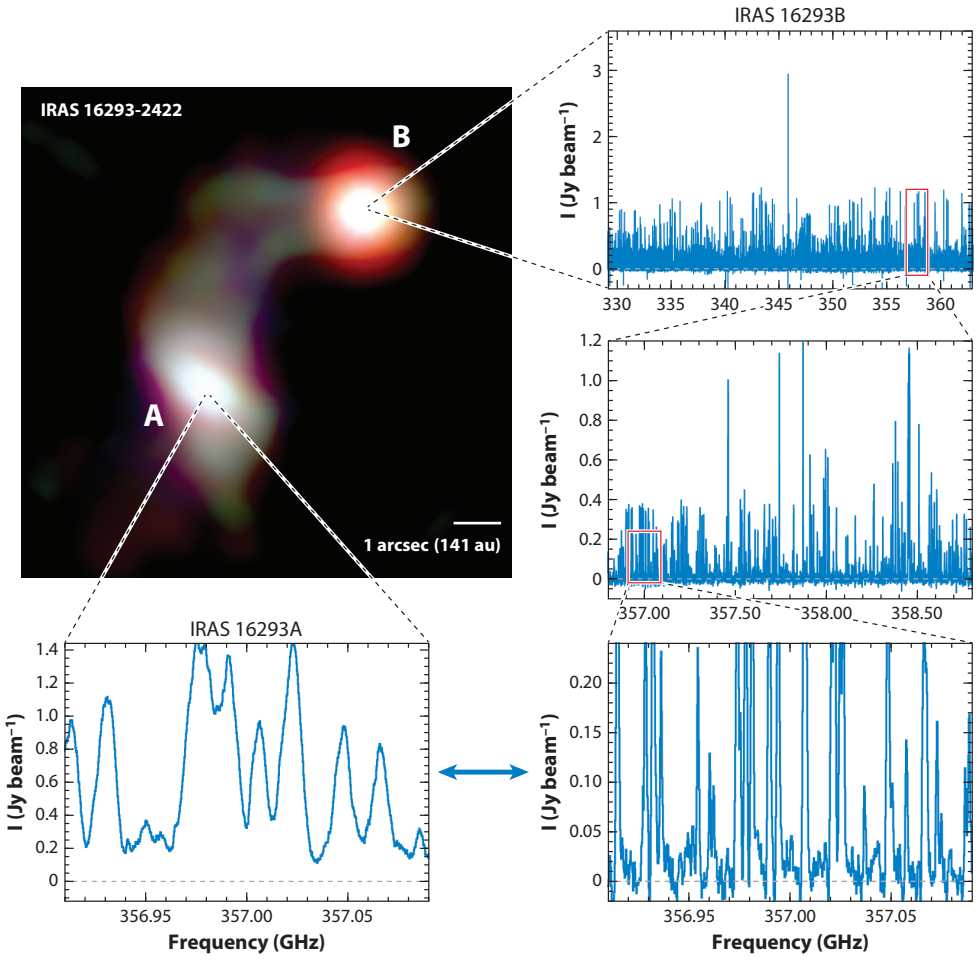

Figure 2

Example of spectra encountered from the ALMA/PILS survey. The image in the top left corner shows the dust continuum radiation from the protostellar binary with the edge-on oriented IRAS 16293A source (*A*) and face-on oriented IRAS 16293B source (*B*) at wavelengths of 3.0 mm (*red*), 1.3 mm (*green*), and 0.8 mm (*blue*). The different orientations cause the line widths to differ significantly for the two sources (≈1 km s^{-1} for IRAS 16293B and ≈5 km s^{-1} for IRAS 16293A). The panels in the right-hand column show spectra progressively zooming in from the full range covered in the survey toward IRAS 16293B. The most zoomed-in version is compared with the same spectrum for IRAS 16293A, illustrating the enhanced line confusion at those scales due to the wider lines of that source. For reference, the RMS noise levels in the spectra are 8–10 mJy $beam^{-1}$, thus most of the features seen represent significant line emission. Data from Jørgensen et al. (2016). Abbreviations: ALMA, Atacama Large Millimeter/submillimeter Array; au, astronomical unit; PILS, Protostellar Interferometric Line Survey.

in the laboratory to measure the rotational spectra of molecules, in particular, complex ones (e.g., Wehres et al. 2018a, Cernicharo et al. 2019).

The challenges with such wide spectral scans lie mainly in dealing with huge data volumes and in the need for new tools for their analysis. Previous more targeted, and lower sensitivity, studies typically only picked up (at most) some handfuls of lines of an individual species. In those cases classical rotation diagram methods worked well, because one could deal practically with

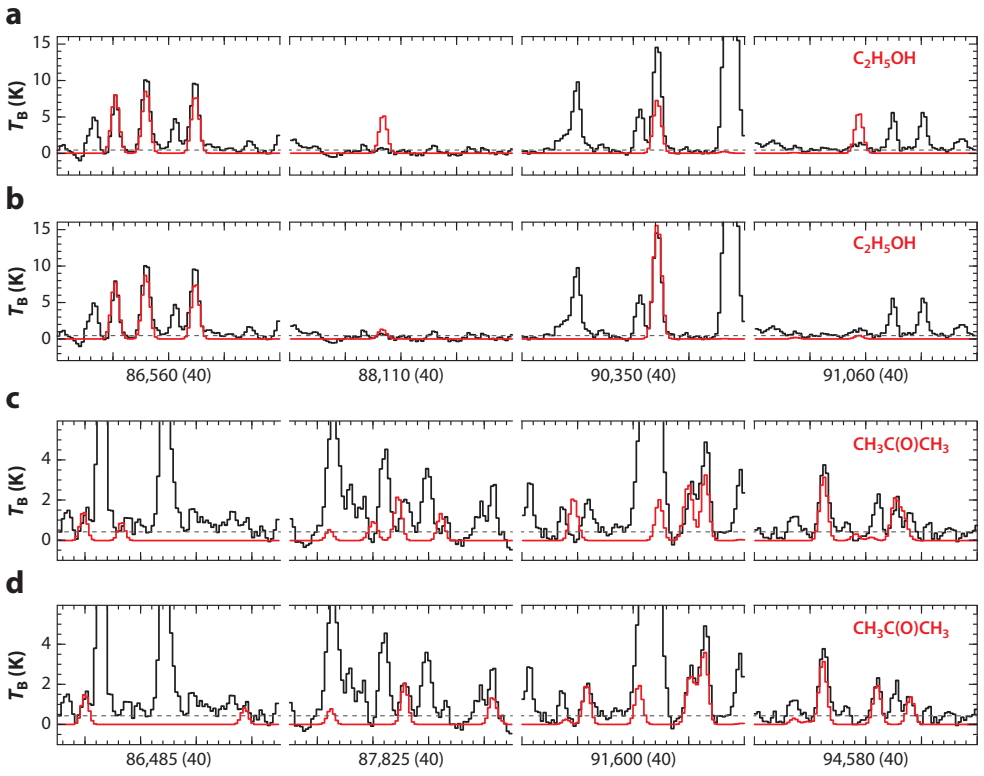

Figure 3

Synthetic spectra (*red*) of (*a*,*b*) ethanol and (*c*,*d*) acetone computed assuming local thermodynamic equilibrium, overlaid on spectra (*black*) of the hot molecular core Sgr B2(N2) observed with ALMA in the frame of the EMoCA project. The synthetic spectra of panels *b* and *d* were computed with recent spectroscopic predictions produced by Müller et al. (2016a) and Ordu et al. (2019), respectively. They agree much better with the observed spectra than the synthetic spectra computed with older predictions from the Jet Propulsion Laboratory database (panels *a* and *c*). The central frequency and frequency range (in parentheses) are indicated in megahertz below each subpanel. Data from Belloche et al. (2016). Abbreviations: ALMA, Atacama Large Millimeter/submillimeter Array; EMoCA, Exploring Molecular Complexity with ALMA.

separating and fitting individual lines. However, in the larger, typically more confused, spectra, it is often more useful to fit the entire observed spectrum using synthetic models (see **Figure 3** for examples). Such models predict the full spectra under, e.g., the LTE assumption, taking into account optical depth of individual lines specifically, and accounting for multiple molecular species at once, thus implicitly sorting out chance alignments, line blends, and, also importantly, testing for nondetections (see also Section 2.2).

2.1.2. Improvements in sensitivity. Another important aspect of the telescope advances with *Herschel* and ALMA has been the significant improvements in sensitivity, due to both the increased collecting area compared to previous facilities as well as (for ALMA) the excellent conditions on the telescope site. This improvement enables more statistical approaches to astrochemical studies, whether in terms of the ranges of lines and species observed for individual sources or in terms of targeting larger samples of sources. In particular, the latter makes it possible to determine the

degree to which variations in molecular emission signatures for different sources are caused by the influence of, e.g., physical conditions (the impact of the external radiation field, variations in cosmic-ray flux, degree of turbulence, etc.) on the resulting chemistry.

Moving into this new sensitivity regime also brings new challenges. One example is that the line-confusion limit is now reached also for sources that were relatively line-poor in shallower surveys. A spectrum has reached the confusion limit when emission from spectral lines is detected in basically every single spectral channel [see, e.g., the 1.3-mm single-dish spectra toward Sgr B2(N) of Belloche et al. 2013], implying that a longer integration time with the same telescope would not bring any new information. This issue becomes more severe at higher frequencies because the spectral line density of a mixture of COMs is expected to be relatively uniform in frequency space. The line width in frequency space is, however, increasing with frequency (in astronomical spectra the line width is expected to be constant in velocity space) and therefore the likelihood of line overlaps, and thereby confusion, in line-rich sources increases with frequency as well.

Reaching the confusion limit raises some practical problems: In particular, if the observed angular resolution is coarse compared to the kinematical structure of the source, then it becomes difficult, if not impossible, to estimate the underlying continuum emission (see, e.g., *bottom left panel* of **Figure 2**). Rather than subtracting the continuum based on line-free channels before performing Fourier transforms and cleaning of the interferometric data, one needs to either take the continuum into account in the synthetic spectrum modeling or define the continuum by fitting the flux distributions pixel by pixel in the imaged datacubes (see Sánchez-Monge et al. 2018 and Jørgensen et al. 2016 for example methodologies). Although the former has the advantage of most closely resembling the actual data with minimum tinkering, it is often impractical. This is particularly true if the spatial distribution of molecular line emission is considered for line-rich sources.

Several strategies can be adopted to beat the spectral confusion limit in order to detect species that have a low abundance or weak lines. Observations at higher angular resolution can reveal regions with smaller velocity dispersion or separate sources that have different systemic velocities and were blended in larger beams. This strategy led to significant advances, for instance, in Sgr B2(N) (Belloche et al. 2016, 2019) or IRAS 16293 (Jørgensen et al. 2016). Finding sources with intrinsically narrow line widths is another promising avenue that is illustrated, for example, by the recent detection of methoxymethanol[3] in the hot core MM1 of NGC 6334I (McGuire et al. 2017).

Finally, going to lower frequency, where the spectral confusion is less severe, is another option, provided that the emission lines are still strong enough to be detected. IRAM has started to explore frequencies below 80 GHz (down to 70 GHz with NOEMA and 73 GHz with the 30-m telescope), and Bands 1 and 2 of ALMA will be valuable in this respect in the near future. COMs have been detected at even lower frequencies, for instance, propanal and benzonitrile with the Green Bank Telescope (GBT; Hollis et al. 2004b, McGuire et al. 2018). Although confusion is not (yet) an issue at these low frequencies, the difficulty lies in the excitation of the molecules that does not follow LTE in the environments probed by these observations. Collision rate coefficients are not available for many COMs, making a reliable estimate of their column densities under such conditions a challenge. However, recent progress has been made in this respect for, e.g., methyl formate and methanimine (Faure et al. 2014, 2018).

2.1.3. Increased spatial resolution. ALMA has clearly pushed observations at submillimeter wavelengths to a new regime with its high angular resolution and sensitivity providing images

[3] See **Table 1** for a list of the names and formulae for molecules discussed in this review.

Table 1 List of molecules discussed in this review having more than three atoms

Species	Formula	Species	Formula
Acetaldehyde	CH_3CHO	Glycolonitrile	$HOCH_2CN$
Acetamide	$CH_3C(O)NH_2$	Glyoxal	$HC(O)CHO$
Acetic acid	CH_3COOH	Hydroxylamine	NH_2OH
Acetone	$CH_3C(O)CH_3$	Isocyanic acid	$HNCO$
Ammonia	NH_3	Methane	CH_4
Benzene	$c\text{-}C_6H_6$	Methanimine	CH_2NH
Benzonitrile	$c\text{-}C_6H_5CN$	Methanol	CH_3OH
Butyl cyanide	C_4H_9CN	Methoxymethanol	CH_3OCH_2OH
Cyanoacetylene	HC_3N	Methyl acetylene	CH_3CCH
Cyanodiacetylene	HC_5N	Methyl amine	CH_3NH_2
Cyanoformaldehyde	$NCCHO$	Methyl chloride	CH_3Cl
Cyanomethanimine	$NHCHCN$	Methyl cyanide	CH_3CN
Cyanomethyl radical	CH_2CN	Methyl formate	CH_3OCHO
Cyclopropenone	$c\text{-}H_2C_3O$	Nitrous acid	$HONO$
Dimethyl ether	CH_3OCH_3	Propanal	C_2H_5CHO
Ethanimine	CH_3CHNH	Propanol	C_3H_7OH
Ethanol	C_2H_5OH	Propenal	C_2H_3CHO
Ethyl cyanide	C_2H_5CN	Propyl cyanide	C_3H_7CN
Ethylene glycol	$(CH_2OH)_2$	Propylene oxide	$c\text{-}CH(CH_3)CH_2O$
Formaldehyde	H_2CO	Quinoline	C_9H_7N
Formamide	NH_2CHO	Thioformaldehyde	H_2CS
Formic acid	$HCOOH$	Vinyl cyanide	C_2H_3CN
Glycolaldehyde	$CH_2(OH)CHO$	Urea	$NH_2C(O)NH_2$

of dust and gas with a resolution of 0.01 arcsec, corresponding to scales of a few astronomical units in nearby star-forming regions. Even in ALMA's intermediate baseline configurations, the achieved angular resolution of ≈0.1 arcsec represents an improvement by a factor of 5–10 in angular resolution compared to what is typically achieved at other facilities. Besides helping with issues such as line confusion described above, the advantages of imaging at these spatial scales are obvious: It makes it possible to look at the spatial coincidences and separations between different species and thereby reveal their chemical relations and their link to the underlying source physical structures.

One challenge encountered in high-resolution studies of low- and high-mass protostars comes from the optical thickness of the observed line and continuum emission. Many sources show unresolved continuum structures that become optically thick, in particular, in the higher-frequency ALMA bands. The continuum optical thickness may, for example, suppress the line emission on protostellar disk scales (e.g., Harsono et al. 2018). These effects made it necessary for the PILS and Re-exploring Molecular Complexity with ALMA (ReMoCA) surveys to focus on positions offset from the main continuum peaks to derive reliable column densities.

2.2. Spectroscopic Identifications of New Species

There are a number of considerations to make when reporting detections of new species or presenting derivations of their physical/chemical characteristics. This is becoming particularly important with the new sensitive observations, where line-rich spectra of individual sources are often revealed serendipitously.

2.2.1. Considerations for new detections. Although it may be uncontroversial to report the detection of a common species toward sources belonging to a well-studied group, more care needs to be taken with an exotic claim (such as a completely new species or the detection of a species toward a type of region in which it has not previously been seen). In the former case, it is often sufficient just to note the rest frequency of the species from common spectroscopic references, but in the latter case a range of transitions is required to be measured independently. The number of transitions needed for a secure claim strongly depends on the spectral line density (see Neill et al. 2012, Halfen et al. 2006).

For new detections, a number of other criteria should be fulfilled as well: The line widths and local-standard-of-rest (LSR) velocities of all transitions of a given species have to be consistent or, if they vary (for example, as a function of energy level), an explanation needs to be provided (obviously an interesting scientific result in its own right). Likewise it is critical to check that the column density and/or excitation temperature derived based on the measured transitions do not predict other transitions to be present across the observed spectral ranges where they are not seen, e.g., from lines of higher intrinsic strengths or more favorable energy levels. Chance alignments from transitions of other (more common) species should also be checked. In particular, in the ALMA era it is often found that even fairly high energy levels of common organic molecules can be populated (including rotational levels in vibrationally or torsionally excited states) that can lead to serious false identifications. To fulfill all these criteria, especially in the case of hot cores or corinos, a recommended approach is to fit a complete spectral survey with a synthetic spectrum that accounts for all identified molecules rather than rely on simple independent Gaussian fits of individual lines of a given species. The formalism behind such synthetic spectra is described by Möller et al. (2017), and a number of publicly available tools are available to calculate them (e.g., `CASSIS`, `XCLASS`, `Weeds`, and `MADCUBA`). Details about basic radiative transfer equations and the derivation of column densities can be found in, e.g., Goldsmith & Langer (1999) and Mangum & Shirley (2015).

An often overlooked aspect is the impact of continuum emission on small scales: The presence of high column densities of dust on small scales can introduce frequency-dependent continuum opacity, significantly altering the intensities of observed molecular transitions if split over multiple bands. The strength of the continuum emission may also be such that the corresponding background temperature terms in the equation of radiative transfer cannot be neglected (see, e.g., section 4.4 of Belloche et al. 2019). Also, these effects strongly affect the use of traditional methods such as population diagrams that typically assume a negligible amount of background radiation (see Goldsmith & Langer 1999 for details about population diagrams).

Finally, the spectroscopic reference needs to be evaluated in terms of the accuracy of the listed frequencies and any extrapolations from laboratory measurements (see **Figure 3** and Section 2.2.3). We encourage astronomers to inspect the documentation for individual species in the spectroscopic databases such as the Cologne Database for Molecular Spectroscopy (Müller et al. 2001, 2005) and the Jet Propulsion Laboratory's database for molecular spectroscopy (Pickett et al. 1998) and cite the relevant spectroscopic studies, and spectroscopists to make their measurements and associated predictions as well as partition functions in such databases available in order to increase the impact of their work in the astrochemical community.

2.2.2. Reporting physical properties. In the contexts of both new detections and when reporting properties from line emission for other species, there is also a range of issues that need to be considered and reported. Exact positions, beam sizes, and, in the case of interferometric observations of extended structures, spatial sensitivity—in terms of (u, v)-coverage—obviously belong to such critical information. For constraints on the column densities of the emission, it is important

to consider the source size in comparison to the angular resolution of the observations. In mapping observations, this involves a comment about the distribution of the material (i.e., whether it is Gaussian or homogeneous with respect to the beam) and whether the column density is estimated from a single position or pixel (where the measured flux density in janskys per beam can be translated into an effective radiation temperature in kelvins) or whether an integration over a larger area is adopted (where the beam-to-pixel size ratio also needs to be taken into account).

As mentioned above, when constructing a model for the excitation of a given molecule, the important physical parameters besides the column density and excitation temperature are the systemic velocity and line width. In particular, the latter—together with the assumed extent—is important when considering possible optical depth effects. On the scales routinely probed with ALMA, many lines of the main isotopologues (and in some cases even less abundant isotopologues; Jørgensen et al. 2018) become optically thick. In those cases, it is often possible to obtain apparently good fits in population diagrams, but if those lines in reality are optically thick, then no constraints are obtained on the actual column densities. For such species it is therefore critical to seek additional constraints to confirm which lines are optically thin—by either looking at rarer variants or studying transitions with lower line strengths—when constraining their column densities.

It is also important to consider whether or not LTE is a reasonable approximation, i.e., whether the densities of the main collision partners (typically H_2) in the region are sufficiently high that the excitation of a molecule is collision-dominated. In hot corinos and cores in which the densities exceed 10^7–10^8 cm^{-3}, LTE is often achieved for most species and transitions of interest, but in more tenuous environments (e.g., prestellar and translucent cores, outflow regions) this is not necessarily the case. It is also worth keeping in mind that while LTE may work well at high frequencies (e.g., at submillimeter wavelengths) for a given source, this may not be the case for the same source at lower frequencies (e.g., centimeter wavelengths) if the observations trace more extended emission. In the case of non-LTE excitation it becomes even more problematic to trust the assignments of lines and thus claims of detections and properties of a given species. This issue may outweigh the advantage that the line confusion at longer wavelengths may be lower.

For species excited to temperatures of 100–150 K or above it is important to note whether the partition function associated with a given spectroscopic entry includes the vibrational contribution or whether it is purely rotational. In the latter case, vibrational corrections need to be applied to derive the full column density of the molecule (see, e.g., section 5 of Margulès et al. 2017).

A final consideration is whether column densities or abundances are reported for the modeled species. Abundances are very often referenced relative to the column density of H_2, as estimated from the dust continuum or CO gas-phase lines. However, such estimates may be problematic (e.g., due to different spatial distributions of CO and the targeted species) or highly model-dependent (e.g., the dust temperature and assumed dust opacity law). Often it is helpful to focus on the relation between a given species and its possible chemical precursor, but again here care must be taken that the choice of reference species does not introduce spurious correlations, e.g., due to assumptions about the excitation or the line optical thickness of the reference species.

2.2.3. The importance of laboratory spectroscopy. The identification of interstellar COMs rely heavily on the accuracy of frequencies and line strengths derived from the analysis of laboratory measurements (see the review by Widicus Weaver 2019). The complexity of the COM Hamiltonians due to, e.g., internal rotation, makes extrapolations beyond the range of frequencies measured in the laboratory uncertain or even unreliable. With the new era of sensitive spectral broadband data sets at submillimeter wavelengths, laboratory measurements at high frequencies are becoming even more crucial. The spectroscopy community has already begun to extend the

spectral characterization of a number of COMs into the submillimeter domain (e.g., Kolesniková et al. 2018, Wehres et al. 2018b, Motiyenko et al. 2019). But even the extension of the spectroscopy of COMs from the centimeter range, investigated several decades ago, to the millimeter range already represents significant progress (e.g., Alonso et al. 2016, Cernicharo et al. 2016, Martin-Drumel et al. 2019).

Radical: a molecular species that has an unpaired valence-shell electron, making it typically very reactive

A more accurate characterization of the Hamiltonian of COMs with advanced modeling codes is also critical: The identification of new interstellar COMs with low abundance requires a good knowledge of the complete spectra of more abundant, known, COMs—that is, not only their strongest lines but also the weaker ones. The recent progress made with, for example, C_2H_5OH (e.g., Müller et al. 2016a) or $CH_3C(O)CH_3$ (e.g., Ordu et al. 2019) illustrates how critical this is (see **Figure 3**). There is also a strong need to characterize the rotational spectrum of COMs in their vibrationally excited states (e.g., Müller et al. 2016b, Degli Esposti et al. 2017), and of their isotopologues (e.g., Margulès et al. 2016, Zakharenko et al. 2019), to advance the line identification of astronomical spectra.

2.3. Linking Observations, Chemical Modeling, and Laboratory Experiments

Our understanding of the chemistry of star-forming regions is constantly informed by ongoing efforts to simulate it both in the laboratory and through computational means. The latter includes the calculation of both rates and parameters of individual processes and full-scale chemical kinetic simulations of astronomical objects. However, observational discoveries of new molecules have often been the driving factor in the choice of species to study.

Over the past decade or so there has been an increased interest in determining the importance, or otherwise, of dust grain-surface chemistry to the production of COMs, including through thermal or energetic processing of mixed molecular ices, as well as their relative importance compared to, e.g., gas-phase processes. Although the field has largely moved beyond the facile "either/or" argument, there is nevertheless still disagreement as to the precise origins of even some of the most commonly observed molecules in star-forming regions, such as formamide (NH_2CHO). Quantum rate calculations for the gas-phase reaction of formaldehyde (H_2CO) with the radical NH_2, leading to formamide, have suggested variously that this mechanism is very efficient (Barone et al. 2015, Skouteris et al. 2017) or that it is prohibitively inefficient (Song & Kästner 2016). Meanwhile, chemical models indicate (e.g., Garrod 2013, Quénard et al. 2018) that with warm (~20 K) dust grains, formamide can be produced through reactions within/upon the ice mantles. Even for molecules such as dimethyl ether, with plausible production mechanisms both in the gas phase and on grains (see **Figure 4**), the relative contributions may also be dependent on the interaction of large-scale physical conditions like temperature with molecule-specific microscopic quantities such as binding energies. Thus, it is likely that there is no blanket description that applies equally well to all COMs, even within a single astronomical source. The chemistry of star-forming regions may perhaps be best described as an intrinsically well-coupled gas-grain chemical system. The recent push to explore the limits of both gas and grain-surface/ice chemistry has led to the investigation of a number of new types of reaction mechanisms, which may become standard parts of the toolbox for astrochemical simulations of all kinds.

2.3.1. Chemical modeling. Chemical kinetic models of star-forming regions calculate the time-evolution of chemical abundances, as determined by a network of reactions and processes and their rates. The main advances made in this field over the past decade involve either the improvement or expansion of chemical networks, the detailed treatment of grain-related chemistry, or the improvement of astrophysical inputs such as density, temperature, and radiation fields.

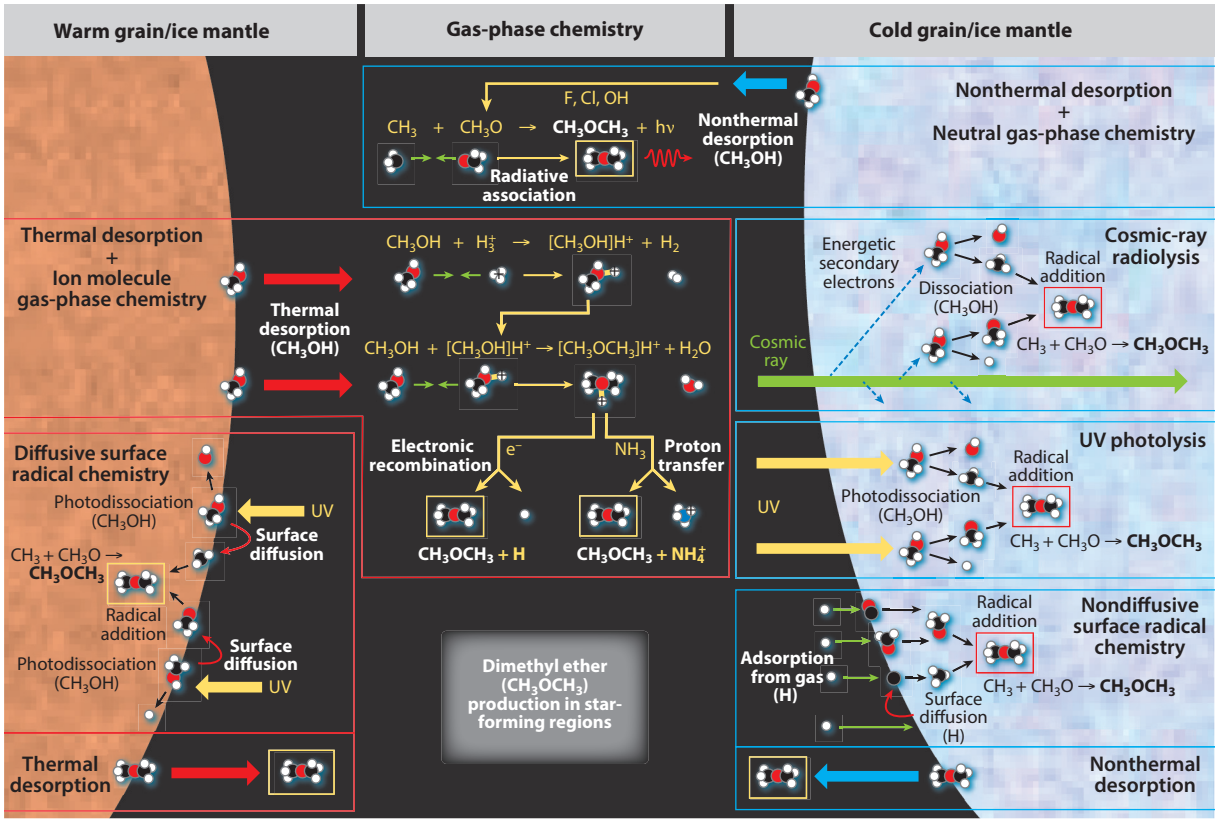

Figure 4

An illustrative selection of proposed pathways to the formation of the representative complex organic molecule dimethyl ether (CH_3OCH_3) in star-forming regions under either warm or cold conditions. Not all possible pathways are shown. Each of the processes occurring on cold grains or within cold ice mantles could also occur at higher temperatures, although with arguably lower significance. The warm grains should be assumed to inherit much of the ice-mantle composition of the earlier, cold dust grains. The cold UV-induced photolysis process implicitly assumes minimal thermal diffusion of dissociation products. The cosmic-ray radiolysis process could also involve suprathermal dissociation products (not shown). UV photolysis and cosmic-ray-induced radiolysis may occur either within the ice mantles or on their surfaces. On the warm grains, surface diffusion of many radicals is expected to be rapid, but diffusion rates within the ice mantles remain uncertain and could also depend on the presence of ice porosity. Gas-phase protonation of, e.g., methanol may occur by reaction with multiple different molecular ions and not only H_3^+. Electronic recombination of protonated dimethyl ether, $[CH_3OCH_3]H^+$, is expected to produce dimethyl ether in no more than 7% of cases, whereas proton transfer to ammonia (NH_3) may be very efficient.

Models of complex molecule production in star-forming regions have frequently concentrated on high-mass star-forming regions, i.e., hot cores. Since the early models of hot-core chemistry, such as that of Brown et al. (1988), some form of two-stage physical model has been assumed. In those, the first stage involves the low-temperature evolution and/or collapse of a molecular cloud core, with the second treating the hot-core stage proper, with higher densities and temperatures. A major feature of the first stage involves the build-up of molecular ice mantles on dust grains, composed primarily of simple hydrides such as H_2O, NH_3, and CH_4, as well as CO, CO_2, H_2CO, and CH_3OH. In the second stage, these are ejected into the gas phase—either immediately or gradually, according to a time-dependent release as temperatures are ramped up to observed values

(Viti & Williams 1999). The thermal ejection of grain-mantle molecules is a major driver of gas-phase chemistry, through both ion–molecule and neutral–neutral reactions (Charnley et al. 1992).

Photolysis: the process of photodissociation of molecules, and subsequent associated mechanisms, caused by photons typically at UV/visible wavelengths

2.3.2. Grain-surface chemical treatments. Models with some explicit treatment of grain-surface chemistry are now fairly standard, due to the need to consider ice evolution. The use of three-phase models (ice mantle, surface, and gas phase), based on the treatment by Hasegawa & Herbst (1993), has also become more common. These models treat the upper ice layer as a separate phase from the underlying bulk, which in some cases is treated as being chemically active (Garrod 2013). Other models have considered multiple layers within the bulk (Taquet et al. 2014). In general, gas-grain models calculate grain-surface abundances using the same so-called rate equation approach as is used for pure gas-phase chemistry. This method ignores the inherently stochastic nature of the grain-surface chemistry and can lead to divergence from numerically exact treatments. Vasyunin & Herbst (2013a) successfully constructed a three-phase model that treats both gas and grain chemistry accurately using a macroscopic Monte Carlo method, followed more recently by Lu et al. (2018). Rate-equation models can also be adapted to replicate stochastic surface chemistry reasonably well, using the modified-rate method (Garrod 2008, Garrod et al. 2009), although the method has not been widely adopted (Furuya et al. 2015).

Much modeling work over the past decade has involved the development of chemical networks for the grain-surface production of COMs. Early grain chemistry networks (Tielens & Hagen 1982) included mechanisms for the build-up of certain COMs by repetitive atomic addition, as well as through reactions between radicals (Allen & Robinson 1977). Garrod & Herbst (2006) presented a model of hot-core chemistry in which the surface mobility, and thus the reactivity, of radicals on grain surfaces would be enhanced by including the gradual warm-up of the gas and dust, which had previously been considered only in the context of the desorption of grain-surface molecules (Viti & Williams 1999, Viti et al. 2004). In these models, radicals are produced largely as the result of photodissociation (i.e., photolysis) of stable, solid-phase species such as methanol (CH_3OH), caused by cosmic-ray-induced UV photons. Reactions between the radical products of methanol dissociation become prominent at temperatures of 20–40 K, resulting in the subsequent formation of many COMs. Many of those linger on grain surfaces until temperatures upward of 100 K are reached, where they sublimate and become observable in the gas phase. The models were expanded to include a larger network of radical reactions (Garrod et al. 2008) that was quite successful in providing a basic framework for the production of many COMs, which has been extended over subsequent years to include newly detected species (Müller et al. 2016a, Belloche et al. 2017, Garrod et al. 2017), especially toward Sgr B2(N).

Importantly for gas-grain models, uncertainties exist in the desorption energies (i.e., binding energies) and diffusion barriers of many chemical species. The former control the temperatures at which atoms or molecules may thermally desorb from the dust grains and into the gas, whereas the latter determine the rates at which reactive species may migrate on the grain surfaces through diffusion, allowing them to react (see also Cuppen et al. 2017). In the case of radicals, both values are often poorly defined by experiment, due to these reactive species' short lifetimes. Some grain-surface reactions require a chemical activation energy barrier to be overcome. Below ~100 K, many such processes important to astrochemistry involve quantum tunneling of H atoms; however, the rates for barrier-mediated reactions used in chemical networks are often poorly defined. Hydrogen addition to unsaturated COMs, which often involves an activation barrier, could be especially important to interstellar abundances (Álvarez-Barcia et al. 2018, Krim et al. 2018).

The degree of diffusion that can occur within the bulk ice is also uncertain and could indeed be minimal for species other than H and H_2. Although such diffusion is technically required in the models to allow radical photoproducts to react within the bulk, new methods are emerging to

Radiolysis: the ionization, and subsequent associated processing, of a target material caused by the impingement of an ionizing particle

treat those reactions without mediation by diffusion, allowing COMs to be formed even at very low temperatures (Garrod 2019), which is in line with experimental evidence (e.g., Henderson & Gudipati 2015).

The strength of the radical–radical reaction process for COMs is affected by both the warm-up timescale of the core and the rates of ice photodissociation, which scale with the cosmic-ray ionization rate. These two physical inputs are somewhat degenerate in their chemical effects. Recent models (e.g., Barger & Garrod 2020) indicate that short warm-up timescales (on the order of 10^4 years) and high cosmic-ray ionization rates ($\sim 10^{-16}$ s^{-1}) may provide the best agreement with observations. Dedicated models of chemistry in individual cores within Sgr B2(N) (Bonfand et al. 2019, Willis et al. 2020) support the latter finding. Photodissociation rates of individual solid-phase molecules are also not well constrained by laboratory data, although they are expected to be lower than equivalent gas-phase processes by a factor of a few (Kalvāns 2018).

Shingledecker et al. (2018) presented a gas-grain model of cosmic-ray-induced radiolysis of interstellar ice mantles. In the case of cosmic rays, the impinging particle (which may be an electron, proton, or heavier atomic nucleus) has far more energy than is required to produce a single molecular ionization, and the resultant electron will also be capable of producing further ionization events. The cascade of electrons produced by a single cosmic ray results in dissociation, excitation, ionization, and recombination of species within the ice. Shingledecker et al. considered this process as a means of forming COMs in quiescent interstellar clouds (mostly through reactions between neutral product species, including radicals), but the mechanism could also plausibly influence COM abundances in actively star-forming cores (see also Section 2.3.4).

2.3.3. Gas-phase mechanisms. Gas-phase production mechanisms for COMs have long been a part of the chemical networks, and the production of some relatively complex species through ion-molecule gas-phase chemistry remains uncontroversial. For example, for dimethyl ether, i.e., CH_3OCH_3 (**Figure 4**), the gas-phase reaction of methanol with protonated methanol ($CH_3OH_2^+$) can lead to the formation of protonated dimethyl ether. This species can recombine with an electron to produce dimethyl ether in up to 7% of cases, whereas the remainder of recombinations should result in the fragmentation of the underlying C–O bonds (Hamberg et al. 2010). Chemical models indicate that the large abundances of gas-phase methanol, following grain-mantle ejection, could make this process effective enough to explain dimethyl ether observations in star-forming regions. However, for other molecules, the inefficient conversion of protonated molecules to a stable, neutral COM via electronic recombination presents a problem. The main gas-phase destruction mechanism for many COMs will also be their protonation by small molecular ions, followed by destructive electronic recombination.

Taquet et al. (2016) proposed a solution to this problem, citing the reaction of protonated COMs with gas-phase NH_3 (following its desorption) as a way to remove a proton without destroying the underlying COM structure. They also suggest that gas-phase mechanisms could produce a selection of COMs through ion-molecule chemistry, with proton transfer to ammonia being the terminal step. These authors further proposed that the heating of grains as the result of episodic accretion events in low-mass sources (see Section 5.3) could induce thermal desorption of molecules that would promote gas-phase chemistry. The formation of methyl formate would proceed via the reaction of protonated methanol with formic acid, leading to the *trans*-conformer of protonated methyl formate (Neill et al. 2011). Further conversion to produce the commonly observed *cis*-methyl formate would be required, but the efficiency of the overall process under interstellar conditions is not well constrained.

There has recently been renewed interest in neutral gas-phase reaction mechanisms for COM production (prompted by the detection of cold COMs in prestellar cores), especially those

involving radicals. Such mechanisms include radiative association, a process by which two species react to form a single product that is stabilized by the emission of a photon. These reactions are inefficient for small-molecule production, but for larger products—including COMs—the efficiency could be much greater. Calculations by Vuitton et al. (2012) suggest radiative association is rapid for large hydrocarbon radicals. Vasyunin & Herbst (2013b) found the radiative association reaction $CH_3 + CH_3O \rightarrow CH_3OCH_3 + h\nu$ to be effective under prestellar core conditions. Rates for radiative association are generally difficult to constrain in the laboratory, so detailed calculations will be required to confirm the production efficiencies for specific COMs. Balucani et al. (2015) noted further that the abstraction of a hydrogen atom from dimethyl ether by Cl and, to a lesser extent, F atoms—followed by reaction of the resultant radical with an O atom—could lead to the production of methyl formate itself. Skouteris et al. (2018) recently considered similar processes beginning with ethanol to form glycolaldehyde, and acetic and formic acid. Many of the above-mentioned reactive processes have been tested with chemical models under only a limited set of physical conditions (centered mainly around cold, prestellar core conditions) and are dependent on the efficient gas-phase production of radicals. However, this neutral and radical chemistry provides an important new dimension to networks for COM production, and further investigation will be highly valuable.

2.3.4. Laboratory experiments. The production of COMs through the irradiation of mixed molecular ices has long been an important area of astrochemical research. The relative influence of cosmic-ray-induced UV/visible irradiation (i.e., photolysis) versus direct cosmic-ray impingement (i.e., radiolysis) in interstellar COM production continues to be debated. Complex organics typical of star-forming regions can be produced through either scheme (Bennett et al. 2007, 2011; Öberg et al. 2009; Öberg 2016). However, the action of suprathermal (i.e., excited or kinetically energetic) species may play a larger role in radiolysis, whereas COM production through photolysis would be closer to the radical-addition mechanisms considered in many astrochemical models. Öberg et al. (2009) demonstrated that a large range of observed COMs could be formed through photolysis of solid methanol, with product abundances varying with temperature (20–70 K). More recently, Butscher et al. (2016) showed that HCO radicals produced by formaldehyde photodissociation could be stored in the ice at low temperatures, becoming more mobile and reactive as temperatures increase. The relative orientations of the radicals during reaction may also be important to the product ratios and reaction efficiencies (Bergner et al. 2016, Enrique-Romero et al. 2016, Butscher et al. 2017).

A major area of new ice-chemistry research involves the production of COMs at very low temperatures without the need for diffusion of large radicals (thermally or otherwise), nor with any initiating energetic process. Fedoseev et al. (2015) found that codeposition of H and CO at low temperatures could produce COMs, which they suggest occurs through the production of glyoxal (HCOCHO) via HCO radical addition, which is subsequently hydrogenated to produce glycolaldehyde and ethylene glycol. In this scheme, the low-temperature chemistry that produces methanol by hydrogen addition would allow more complex species to be formed in tandem. Reactions between HCO radicals would be the result not of diffusive meetings but rather of their occasional production in close enough proximity that little or no diffusion would be required. The HCO radical could also plausibly react with CO itself, mediated by an activation energy barrier but with little need to diffuse. Subsequent studies have highlighted cold pathways to other COMs, through deposition of additional species (Fedoseev et al. 2016, Dulieu et al. 2019, Qasim et al. 2019). In this review, we refer to such processes generically as nondiffusive, although they may indeed be initiated by the diffusion of H atoms, which are mobile even at very low temperatures. It seems likely that nondiffusive mechanisms could make a significant contribution to the

COM content of star-forming regions. However, methyl formate does not seem to be produced in sufficient quantities to explain its interstellar abundance, and photolysis may therefore still be required (Chuang et al. 2016) if it originates in the solid phase. Astrochemical models have treated nondiffusive reactions in the past on a case-by-case basis (Garrod & Pauly 2011), but new models are beginning to include more general treatments for this cold chemistry (e.g., Jin & Garrod 2020).

3. CHEMICAL INVENTORIES IN REGIONS OF STAR FORMATION

3.1. Recent Salient Results About Molecular Complexity

Between 2010 and 2019, 58 new species were detected in the ISM, at a rate exceeding the approximately 4 new detections per year on average since 1968 (McGuire et al. 2018). About 36% of those new detections were COMs, of which 71% were detected toward dark clouds or star-forming regions, with the majority being highly saturated species. Since 2014, 6 out of 16, i.e., ∼40% of the new COM detections, were made with ALMA, which was a clear demonstration of its capabilities for astrochemical studies. But large single-dish telescopes still have a role to play, as illustrated by the detections of 9 new COMs with the GBT and IRAM 30-m telescopes over the same period (4 and 5, respectively, for these telescopes).

Three of the new COM detections reported over the past five years have revealed the wider complexity of the molecular structures produced by chemistry in star-forming regions. The ALMA detection of the branched alkyl molecule isopropyl cyanide toward the hot core Sgr B2(N2) with an abundance only 2.5 times lower than that of its straight-chain structural isomer normal-propyl cyanide has shown that branched molecules can easily form in the ISM (Belloche et al. 2014). Astrochemical simulations subsequently showed that at the next stage of complexity in the alkyl cyanide family (C_4H_9CN), some of the branched isomers should even dominate over the straight-chain one (Garrod et al. 2017). This remains to be verified observationally. The detection of a chiral molecule has also enlarged our inventory of the types of molecular structures present in the ISM: McGuire et al. (2016) reported the detection of propylene oxide in the extended, low-density region of the protocluster Sgr B2(N) with the GBT and the Parkes radio telescope. These observations do not tell us if propylene oxide has an enantiomeric excess in Sgr B2, as was found for some chiral molecules in meteorites (see, e.g., Pizzarello & Groy 2011), but McGuire et al. (2016) discuss the prospects for a measurement of this. Finally, the identification of an aromatic COM in the ISM was reported by McGuire et al. (2018), who detected benzonitrile toward the cold dense core TMC-1 with the GBT. Apart from the fullerenes, this molecule is, with 13 atoms, the largest molecule identified in the ISM so far. As those authors' chemical models indicate, its presence is likely connected to the chemistry of benzene. However, it is less clear whether benzene itself should be formed predominantly through a bottom-up mechanism starting from simpler species or whether it represents the smaller end of a spectrum of polycyclic aromatic hydrocarbons that are relatively long lived and photostable.

Attempts to detect larger molecules such as butyl cyanide (15 atoms) or the heterocyclic aromatic molecule quinoline (C_9H_7N, 17 atoms) have not been successful so far (Ordu et al. 2012, Cordiner et al. 2017, Garrod et al. 2017). Garrod et al. (2017) predicted an abundance of butyl cyanide relative to propyl cyanide in Sgr B2(N) just below the detection limit of the EMoCA survey, but a preliminary search for this molecule in the three times more sensitive survey ReMoCA on the same source (Belloche et al. 2019) has not been successful yet. Likewise, no secure detection of propanol (12 atoms) has been achieved so far (Tercero et al. 2015, Müller et al. 2016a, Qasim et al. 2019).

3.2. Detections in the Warm Gas of Hot Cores and Corinos

Through efforts with ALMA, *Herschel*, and other millimeter/submillimeter facilities, significant advances have been made toward the collection of systematic molecular inventories for a larger number of sources, including those that are generally less line-rich. For example, many of the complex species previously only detected toward high-mass star-forming regions are now also seen toward solar-type protostars. These include molecules containing three carbon atoms, such as acetone and propanal (Lykke et al. 2017), and species of prebiotic interest such as glycolaldehyde (Jørgensen et al. 2012, Coutens et al. 2015, Taquet et al. 2015) and formamide (Kahane et al. 2013, Coutens et al. 2016).

At the current level there is no evidence that the degree of molecular complexity is any less for low-mass hot corinos than their high-mass counterparts, although the former typically have fainter lines. This is not to say that there are no differences between low- and high-mass star-forming regions. There are significant nondetections in some regions: For example, species such as methylamine, CH_3NH_2, and hydroxylamine, NH_2OH, have been sought due to their potential roles as precursors for amino acids. However, so far only CH_3NH_2 has been detected in the ISM and only toward a few select regions such as Sgr B2(N) (Kaifu et al. 1974), Orion KL (Pagani et al. 2017), G10.47+0.03 (Ohishi et al. 2019), and NGC 6334 (Bøgelund et al. 2019b), but not in general toward high-mass star-forming regions or low-mass protostars (Ligterink et al. 2015, 2018a). No secure detection of NH_2OH has been reported so far despite dedicated searches toward high- (Pulliam et al. 2012) and low-mass star-forming regions (McGuire et al. 2015, Ligterink et al. 2018a). An analysis of the PILS data shows that the CH_3NH_2 upper limit as well as the detection of methanimine (CH_2NH), a precursor species of CH_3NH_2, imply abundances with respect to methanol and formamide more than an order of magnitude lower in IRAS 16293B compared to Sgr B2(N) (Ligterink et al. 2018a).

Conversely, the targeted studies of solar-type protostars have revealed the presence of some species not previously seen toward high-mass star-forming regions, for example, the simple halogen-bearing organic methyl chloride (Fayolle et al. 2017), and nitrous acid (Coutens et al. 2019). Due to high degrees of line confusion typically seen toward high-mass star-forming regions, it is not clear whether those species differ in abundance compared to high-mass star-forming regions, as the increased line confusion toward Sgr B2(N2) in the EMoCA survey produces upper limits on the abundance of these two species comparable with the inferred values in IRAS 16293B. Another recent example of a first discovery in low-mass protostars is that of glycolonitrile. This species was detected in IRAS 16293B (Zeng et al. 2019) but searches for it toward Sgr B2(N) have been unsuccessful so far, in both single-dish surveys (Margulès et al. 2017) and the EMoCA and ReMoCA interferometric surveys.

3.3. Low-Density Environments and Starless/Prestellar Cores

Some particularly interesting observations of complex molecules and related species involve detections toward cold starless or prestellar cores. While unsaturated carbon chains have long been known to be present toward such cores (TMC-1 and L134N being the most well-studied examples), recent studies have also yielded detections of a number of saturated COMs toward dense, low-mass prestellar cores such as L1689B in the Ophiuchus molecular cloud region (Bacmann et al. 2012), L1544 in Taurus (Vastel et al. 2014, Jiménez-Serra et al. 2016) and Barnard 5 in Perseus (Taquet et al. 2017), as well as their likely counterparts for high-mass stars such as the IR dark cloud IRDC 028.34+0.06 (Vasyunina et al. 2014) and the prestellar core candidate W43-MM1/6 (Molet et al. 2019). Detected molecules include acetaldehyde, methyl formate,

and dimethyl ether. Maps of the spatial distributions of these species toward some of the cores (Bizzocchi et al. 2014, Soma et al. 2015) suggest that they are prevalent in regions offset from the center of the core as traced by the submillimeter continuum radiation or IR extinction.

The detections of COMs in absorption toward Sgr B2(N) also provide insight into the chemistry of cold clouds. Some of these detections correspond to the large-scale envelope of Sgr B2(N) itself, but a few COMs (CH_3OH, CH_3CN, CH_3CHO, and NH_2CHO) were also detected at velocities corresponding to translucent clouds along the line of sight, both in the Scutum arm and in the Galactic Center region (Corby 2016; Thiel et al. 2017, 2019). The abundances of CH_3CN, CH_3CHO, and NH_2CHO relative to methanol were found by Thiel et al. (2017) to be similar to those derived for the same molecules detected in absorption in the $z = 0.89$ spiral galaxy located in front of the quasar PKS 1830-211 (Muller et al. 2011, 2013). This suggests that the processes leading to chemical complexity in the translucent parts of molecular clouds have remained similar since the Universe was half its current age.

The detections of COMs in these cold regions emphasize two points: First, the formation of these highly saturated organics cannot be dependent on the same warm, diffusive, grain-surface chemistry that many models rely on to explain COMs in hot-core regions. Second, if they originate on the grains, they must be released into the gas through some nonthermal mechanism. Plausible theories include cosmic-ray sputtering of the ices, photodesorption by UV photons, and so-called reactive desorption, in which excited, newly formed molecules spontaneously desorb. However, neither of the latter two mechanisms are found to be efficient for methanol in the laboratory (e.g., Bertin et al. 2016, Martín-Doménech et al. 2016). The presence of COMs in translucent regions, in which photodestruction of those molecules by ambient interstellar UV photons would be more significant, presents a greater problem. Formation of the COMs within transient or unresolved structures (e.g., Garrod et al. 2005) could provide a possible explanation. An alternative idea is that reactions of H and O atoms with the bare surfaces of carbonaceous grains could be a source of COMs. Experiments have, for example, shown that formaldehyde may be produced in this way (Potapov et al. 2017).

These new detections have reset the clock for COM formation to an even earlier stage than previously thought. An important task for the future will be to determine to what degree hot cores and corinos have inherited chemistry from their earlier evolutionary stages.

3.4. Outflows

The first discovery of COMs toward an outflow-related shock was made toward the chemically active outflow L1157-B1 (Arce et al. 2008). This region has since then been the target of unbiased line surveys using the Nobeyama 45-m telescope (Yamaguchi et al. 2012), the IRAM 30-m telescope (Astrochemical Surveys At IRAM or ASAI, Lefloch et al. 2017), and *Herschel*/HIFI (*Herschel*/HIFI spectral survey of OMC-2 FIR 4 or CHESS, e.g., Codella et al. 2010, 2012; Benedettini et al. 2012). These surveys have led to a number of new detections in such shocked regions, including of phosphorus mononitride (PN; Yamaguchi et al. 2011), as well as inventories of COMs there (Sugimura et al. 2011, Lefloch et al. 2017). Beyond the L1157 outflow, the systematic inventories of complex organics beyond CH_3OH and CH_3CN in outflow regions remain relatively sparse. Öberg et al. (2010, 2011) reported the detections of COMs, including CH_3OCHO, CH_3CHO, and CH_3OCH_3, toward outflows in the B1-b and SMM4-W regions with abundances of up to a few percent with respect to methanol. With their relatively rich spectra, the shocks in the L1157 outflow have also been the targets of a number of interferometric studies aimed at searching for chemical differentiation between the various species either between the different shocks or within individual ones (Fontani et al. 2014, Burkhardt et al. 2016, Codella et al. 2017).

Such studies, as well as ones for high-mass protostellar outflows (e.g., Palau et al. 2017), show great potential for observations of chemistry in the time domain that can provide much needed constraints, but naturally require good, independent constraints on the time progression of the shocks as well as the physical changes they induce (e.g., Burkhardt et al. 2019).

3.5. External Galaxies

COMs have also been detected in external galaxies. In Section 3.3, we already mentioned the detections reported in the $z = 0.89$ spiral galaxy in front of PKS 1830-211, with more than 42 simple and complex molecules identified with Australia Telescope Compact Array (ATCA) and ALMA (Muller et al. 2014). Extragalactic detections of methanol, methyl cyanide, and methyl acetylene were already reported three decades ago, in particular in the central regions of the starburst galaxy NGC 253, with abundances similar to abundances in our Galaxy (Henkel et al. 1987, Mauersberger et al. 1991). More recently, hot cores have been reported in the Large Magellanic Cloud (LMC). Shimonishi et al. (2016) identified a hot core toward the high-mass YSO ST11 with ALMA on the basis of its compact size, high density, and high temperature, but no COM was detected, with upper limits implying that methanol is at least one order of magnitude less abundant than it is in Galactic hot cores. Further progress was made by Sewiło et al. (2018), who detected not only methanol but also dimethyl ether and methyl formate toward two hot cores of N113, one of the most prominent star-forming regions in the LMC. The abundances of those species were found to be similar to those found in Galactic hot cores after accounting for the difference in metallicity. Methanol has been detected at even lower metallicity, in a cold core of the Small Magellanic Cloud, with an abundance, not corrected for metallicity, comparable with similar galactic cold sources, which may suggest an enhanced production of methanol at low metallicity (Shimonishi et al. 2018), although the implication is somewhat dependent on the assumptions about the dust properties and temperatures used to derive the H_2 column density (Section 2.2.2).

A limited number of gas-grain chemical models of Magellanic Cloud chemistry have been published: Acharyya & Herbst (2018) present an example of a model of hot-core chemistry in these environments. They found that the effects of varied physical conditions, particularly the minimum dust temperature achieved, could be more influential than the metallicity. Unfortunately, the relatively few detections of COMs so far in the Magellanic Clouds do not place strong constraints on the chemical and physical processes at work.

4. CHEMICAL DIFFERENTIATION IN THE ENVIRONMENTS OF STAR FORMATION

The environment of a star-forming region can have a strong impact on its chemistry: The temperature, cosmic-ray ionization rate, radiation field, and timescale of evolution all influence the rates at which molecules are created or destroyed, and possibly introduce chemical differentiation. In turn, the chemical content of a source can be used to infer its physical properties and history. Good examples of these links are the two favorite hot-core regions, the protocluster Sgr B2(N) in the Galactic Center (GC) region and the 20-times more nearby Orion KL region. Both have been targets of broad spectral line surveys over the past four decades to probe their COM content, but their physical characteristics may in fact be very different. Furthermore, other regions of low- and high-mass star formation are starting to show evidence of chemical differentiation through the increased sensitivity, spectral coverage, and angular resolution of current observational facilities (see Section 2). In this section, we therefore focus on the observational relationships between the physical structure in star-forming environments and chemical differentiation.

4.1. Sgr B2(N): The Impact of Cosmic Rays and an Extended Reservoir of Complex Organic Molecules

The GC giant molecular cloud Sgr B2 shows rich chemical diversity, related to both compact hot cores and more extended material in which complex molecules are also present. The fact that high-mass star formation is happening in Sgr B2 has been known for several decades, with the detection of several dozen ultracompact HII regions indicating the presence of a protocluster of young O and B stars (e.g., Gaume et al. 1995). Recently, a large population of several hundred compact, high-density sources in a likely earlier stage of evolution was unveiled with ALMA through their dust continuum emission, with a large fraction of them being interpreted as tracing high-mass YSOs (Sánchez-Monge et al. 2017, Ginsburg et al. 2018). In Sgr B2(N) in particular, three new hot cores have been identified through their molecular line forests with ALMA (Bonfand et al. 2017); all coincide with previously known Class II methanol masers (Caswell 1996), which are exclusively associated with young high-mass stars (Minier et al. 2003, Xu et al. 2008).

Although the global chemical composition of Sgr B2's main sites of star formation, Sgr B2(N) and Sgr B2(M), could be derived from single-dish observations (e.g., Belloche et al. 2013, Neill et al. 2014), significant progress has been made thanks to ALMA's high angular resolution and sensitivity that allowed the chemical composition of the individual hot cores of Sgr B2(N) to be determined and accurate column densities to be derived (Belloche et al. 2016, Bonfand et al. 2017). Through models of the observed COM abundances of Sgr B2(N)'s hot cores, Bonfand et al. (2019) found evidence for a cosmic-ray ionization rate a factor of 50 higher than the canonical value of 1.3×10^{-17} s^{-1} usually assumed for dense gas in the Galactic disk. This is in qualitative agreement with the higher cosmic-ray ionization rate values found for the diffuse medium of the GC region compared to the diffuse medium in the Galactic disk (Indriolo et al. 2015, Le Petit et al. 2016).

Another interesting discussion concerns the thermal history of the region and its impact on the formation of COMs. Dust temperatures measured with *Herschel* are higher in the GC region compared to the Galactic disk. Temperatures of 20–27 K were derived for Sgr B2 (Guzmán et al. 2015), but they may be affected by the feedback of its star formation. A better proxy for the physical conditions that were prevalent during the earlier prestellar phase in Sgr B2 may be G0.253+0.016, a GC molecular cloud with little on-going star formation. Dust temperatures of 19–27 K were measured in this cloud (Longmore et al. 2012). Bonfand et al. (2019) showed that minimum temperatures above 20 K during the collapse history of Sgr B2(N)'s hot cores would not be consistent with their current COM abundances. This discrepancy implies that either the *Herschel* maps are not sensitive to the lowest temperatures at high densities or our understanding of the formation of COMs, and indeed ices of all kinds, in a region like Sgr B2 would have to be revised. Specifically, the retention of CO ice on grains much above 20 K or so is unlikely, rendering even methanol production a challenge, as it has no efficient gas-phase formation mechanism (Garrod et al. 2007). This discussion may also have implications for more local (low-mass) star-forming regions in which the presence of nearby high-mass stars may cause the temperature floor to be elevated (e.g., Jørgensen et al. 2006).

A feature of Sgr B2 that has been known for nearly two decades but has become more prominent in the past one is the presence of COMs distributed on large scales in the cloud, in addition to the COMs present on small (arcsec) scales in the hot cores. GBT detections of $CH_2(OH)CHO$, C_2H_3CHO, C_2H_5CHO, $(CH_2OH)_2$, c-H_2C_3O, NH_2CHO, $CH_3C(O)NH_2$, NCCHO, CH_3CHNH, and NHCHCN in absorption and/or emission with low-excitation temperatures are indirect indications that these molecules are present at low densities and distributed over arcminute scales in Sgr B2 (Hollis et al. 2004a,b, 2006a,b; Hollis 2005; Remijan et al. 2008; Loomis et al. 2013; Zaleski et al. 2013). Mapping observations confirm this with, for example,

emission of CH_3OH, CH_3CN, CH_3CCH, NH_2CHO, CH_3CHO, and HC_5N extending over several arcminutes in maps obtained with the Mopra telescope at 3 and 7 mm (Jones et al. 2008, 2011) and absorption of CH_2CN, CH_3CHO, and CH_3CHNH detected with ATCA at 7 mm over the extent of the background free–free continuum emission (∼10 arcsec; Corby et al. 2015).

The connection between this low-density, colder emission and the hot cores remains unclear. Recently, Li et al. (2017) reported a change in the relative abundances of $CH_2(OH)CHO$ and $(CH_2OH)_2$ over scales of 15 arcmin in Sgr B2 with the Shanghai Tianma 65-m radio telescope with the $[(CH_2OH)_2]/[CH_2(OH)CHO]$ abundance ratio decreasing from the extended, low-density region to the dense regions Sgr B2(N) and Sgr B2(M), where star formation occurs. The recent detections of COMs in cold cores (Section 3.3) suggest that a similar set of physical conditions could be producing such molecules in both environments, although—if formed on dust grains—the mechanism of desorption could be quite different. The action of shocks in GC environments could provide a more substantial ejection of mantles into the gas (see, e.g., Requena-Torres et al. 2006). Recently, ALMA observations revealed a network of filaments on scales of a few tenths of a parsec toward Sgr B2(N) (Schwörer et al. 2019). The kinematics of the filaments show evidence for mass flows toward a central hub where the main hot core, Sgr B2(N1), is located and imply a timescale of 60–300 kyr for the formation of this central hub. Further investigations of the relation between these filaments and both the formation of the high-mass stars and the chemistry in the extended and compact environments may shed more light on these issues.

4.2. Orion KL: Chemical Impact of a Past Explosion

Thanks to its short distance, Orion KL can be studied in greater detail than Sgr B2, and many signs of chemical differentiation have been seen within this source. For example, resolved CARMA (Combined Array for Research in Millimeter-wave Astronomy) observations showed that cyanides peak at different locations from other species such as CH_3OCH_3 and CH_3OCHO (Friedel & Snyder 2008). A differentiation between N-bearing COMs (cyanides and NH_2CHO) and O-bearing COMs (alcohols, CH_3OCH_3, and CH_3OCHO) has also been inferred from differences in their excitation temperatures from *Herschel* observations by Crockett et al. (2015), who found that the former trace hotter gas (200–300 K) than the latter (100–150 K). However, the $CH_3C(O)CH_3$ emission detected with the Plateau de Bure Interferometer (PdBI) resembles more the cyanide emission than that of CH_3OCH_3 and CH_3OCHO (Peng et al. 2013, Feng et al. 2015), two COMs that were found to be strongly spatially correlated (Brouillet et al. 2013). To complicate the situation even further, Favre et al. (2017) demonstrated with ALMA that CH_3COOH and $(CH_2OH)_2$ trace a more compact region located closer to the hot core than other O-bearing COMs. Analyzing a larger sample of O-bearing COMs detected with ALMA, Tercero et al. (2018) confirmed this result and showed that there is in fact a more general spatial segregation between the COMs containing a C-O-C structure and the COMs containing a C-OH bond, the former tracing the compact ridge and the latter the hot core. Tercero et al. (2018) interpret this segregation as resulting from the chemistry being dominated by different radicals in these two regions, methoxy ($CH_3O\cdot$) in the former and hydroxymethyl ($\cdot CH_2OH$) in the latter. One caveat in these discussions is that integrated intensity maps intended to trace a particular transition of a given COM may be contaminated by emission from other species due to the complex velocity structure of the Orion KL region (Pagani et al. 2017). A more reliable method would be to construct column density maps from LTE fits of the spectrum of each pixel (e.g., using the VINE method; Calcutt et al. 2018b).

As already noted, some species show indications of temperatures across the region ranging from about 100 K up to 300–450 K toward the cyanide peak at the northeastern part of the hot core

(Bell et al. 2014). Among the COM detections recently reported in Orion KL, the detection of propyl cyanide is particularly interesting. Both the straight chain (*n*) and the branched (*i*) isomers were detected with ALMA (Pagani et al. 2017). The authors derived an abundance ratio of the *n*- and *i*-isomers that is similar to the one obtained by Belloche et al. (2014) in Sgr B2 but which varies by a factor of 3 (from 2 to 6) across the region. These variations may reveal a nonuniform thermal history across the Orion KL region (Pagani et al. 2017).

Still, significant evidence has emerged that mechanical rather than thermal processes may strongly influence the chemistry of Orion KL. It has long been known that the region shows a prominent wide-angle outflow with a peculiar structure of finger-like filaments in H_2 emission (Taylor et al. 1984), which is possibly the result of an explosive event (Allen & Burton 1993). A recent explanation for this explosion is that embedded radio and IR sources within the cloud were originally part of a multiple young stellar system that violently disintegrated ∼500 years ago as a result of a close dynamical interaction, creating at the same time the wide-angle outflow (e.g., Bally & Zinnecker 2005, Gómez et al. 2005, Zapata et al. 2009, Bally et al. 2017, Luhman et al. 2017). The absence of a self-luminous submillimeter, radio, or IR source embedded in the hot molecular gas and the fact that there are no outflow filamentary structures in the shadow of the hot core pointing away from the explosion center led Zapata et al. (2011) to suggest that Orion KL is not a typical hot core with internal heating by a nascent star but a preexisting dense structure that was heated up from the outside by the gas that was accelerated by the explosion. An alternative explanation (Goddi et al. 2011, Bell et al. 2014) is that the hot core is externally heated due to interaction with the compact SiO outflow driven by source *I* (Plambeck et al. 2009). In either case, the chemistry of the Orion KL "hot core" could thus be dominated by shocks rather than thermal heating by embedded stars, which corroborates earlier suggestions that the hot core is externally heated (e.g., Blake et al. 1996). The context of the explosion may also shed new light on the structure of the Orion KL region: Pagani et al. (2017) argue that the compact ridge, with its narrow velocity dispersion, is located in front of or behind the rest of the region and has not been affected by the explosion yet.

A recent ALMA study by Pagani et al. (2019) presents an interesting case of probing chemistry in a new way in relation to the explosive event. In addition to kinematic evidence pointed out in their previous work (Pagani et al. 2017), elongations found in the channel maps of various simple and complex molecules, which point back toward the explosion center, are interpreted by the authors as the result of these molecules being dragged away by the expanding gas that was pushed out by the explosion (see **Figure 5**). The authors suggest that molecules that do not show such elongations are quickly destroyed in the gas phase after their release from the dust ice mantles, whereas those showing such elongations survive longer. If this interpretation holds true, then the Orion KL region would turn out to be a kind of time-of-flight experiment that would allow us to explore interstellar chemistry in the time domain. This would be a major observational breakthrough.

4.3. Chemical Differentiation in Other Hot Cores

Another avenue to improve our understanding of the formation of COMs in high-mass star-forming regions, complementary to the detailed studies in Sgr B2 and Orion KL mentioned above, is to target large samples of sources and compare their chemical compositions. Bisschop et al. (2007) found that the species (COMs or otherwise) that they detected with the James Clerk Maxwell Telescope toward seven high-mass YSOs were divided into two groups, one tracing hot gas (>100 K) and the other one cold gas (<100 K). Further studies of small (<10 sources) samples of high-mass star-forming regions targeting several COMs have been performed (e.g., Calcutt

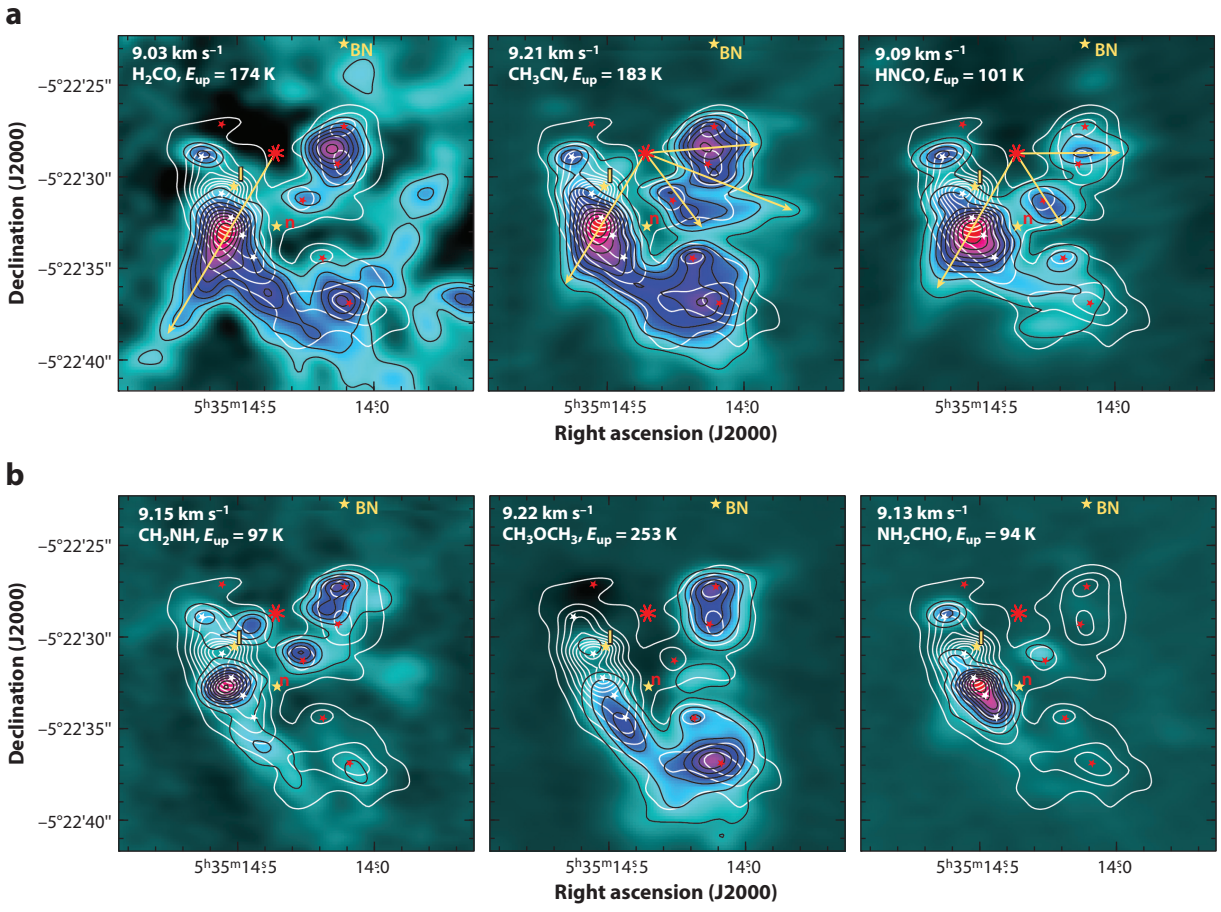

Figure 5

A selection of species seen at 9 km s^{-1} (*color* and *black contours*), compared with the 1.2-mm continuum emission (*white contours*) toward the Orion KL region. The stellar objects BN, I, and n are indicated. Small red or white 5-pointed stars mark IR peaks. The yellow arrows starting from the explosion center (*red eight-pointed star*) suggest possible displacement of gas linked to the explosive event, which occurred ∼500 years ago. The first row (*a*) shows species with conspicuous displacements (from *left* to *right*: H_2CO, CH_3CN, HNCO), whereas the second row (*b*) shows species close to their production sites (from *left* to *right*: CH_2NH, CH_3OCH_3, NH_2CHO). Figure prepared by L. Pagani based on data taken from Pagani et al. (2019).

et al. 2014, Suzuki et al. 2018, Taniguchi et al. 2018), but the lack of angular resolution, the inhomogeneity of the spectral coverage, or the small number of investigated COMs have prevented the emergence of a clear chemical pattern from these studies. Hernández-Hernández et al. (2014) targeted 17 hot cores in CH_3CN with the SMA and found a correlation between the CH_3CN abundance and its rotational temperature, which they interpreted as evidence for a gas-phase formation of CH_3CN. Öberg et al. (2014) argued that the observed increase of [CH_3CN]/[CH_3OH] with temperature could make this ratio an evolutionary tracer of massive YSOs.

In addition to Orion KL, chemical differentiation between N- and O-bearing COMs has previously been reported in W3, W75N, W51e1/e2, and G19.61-0.23 (e.g., Wyrowski et al. 1999; Remijan et al. 2004; Kalenskii & Johansson 2010; Qin et al. 2010, 2015). More recently, ALMA observations revealed a chemical differentiation on small scales (a few 100 au) toward the young

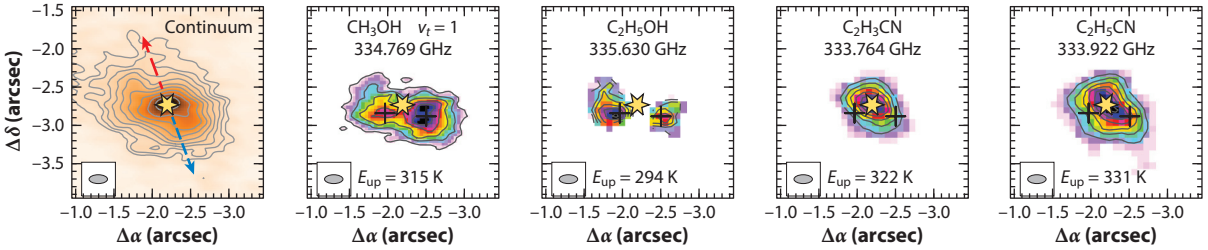

Figure 6

Continuum emission (*far left panel*) and integrated intensity maps of transitions of several complex organic molecules (*other panels*) toward the young high-mass protostar G328.2551–0.5321 obtained with ALMA. Methanol and ethanol trace two spots (*black crosses*) offset from the protostar (*yellow star*) that have velocities consistent with rotation around the outflow axis (*blue* and *red arrows*). In contrast, the emission of vinyl and ethyl cyanide peaks on the protostar. Figure prepared by T. Csengeri based on data taken from Csengeri et al. (2019). Abbreviation: ALMA, Atacama Large Millimeter/submillimeter Array.

high-mass YSO G328.2551–0.5321, with the N-bearing COMs peaking toward the protostar and the O-bearing COMs toward two spots offset from the protostar (Csengeri et al. 2018, 2019). The authors interpreted these two spots, which have velocities consistent with a rotation pattern, as tracing accretion shocks onto a disk (see **Figure 6** and Section 5.1). Chemical differentiation on scales smaller than 1,000 au was also reported by Allen et al. (2017) among the four continuum peaks detected with ALMA toward G35.20-0.74N, but a scenario to explain this differentiation is still lacking.

Determining spatially resolved abundance profiles of COMs in protostellar envelopes is a means to test the predictions of chemical models in order to identify their formation routes. For instance, the spatially resolved analysis of the emission of CH_3OH, CH_3CN, and CH_3CCH toward the massive YSO NGC 7538 IRS9 revealed a change in COM chemistry at temperatures above 25 K, likely reflecting the onset of an efficient ice chemistry above this temperature (Öberg et al. 2013). Such spatially resolved studies of COMs should be generalized toward samples of YSOs in the future. Another strategy is to study families of molecules, such as isomers, in targeted observations of large samples of sources. For instance in the case of the $C_2H_4O_2$ family, El-Abd et al. (2019) found a bimodal column density distribution of glycolaldehyde (GA) with respect to methyl formate (MF), whereas acetic acid correlates uniformly well with the latter. The sources with a high MF/GA ratio are exclusively high-mass objects while both high-mass and low-mass objects populate the region with low MF/GA ratios (El-Abd et al. 2019), similar to comets and quiescent clouds (Rivilla et al. 2017). The reason for this bimodal distribution is not currently understood: A difference in the balance between UV-driven ice processing and other mechanisms, such as cold, nondiffusive, surface chemistry, may provide one plausible explanation (see Section 2.3.4). Further observational and astrochemical modeling studies are required to investigate this discrepancy and the underlying physical mechanisms.

4.4. Spatial Differentiation in IRAS 16293-2422

Chemical differentiation can also be resolved in solar-type regions. Imaging observations of IRAS 16293-2422 indicate some spatial differentiation between N- and O-bearing complex organics (see Bisschop et al. 2008). However, also within these groups of different complex organics, systematic differences can be seen toward one of the two components in the system, IRAS 16293A: Toward this source a number of species, including HNCO, H_2CO, $CH_2(OH)CHO$, $(CH_2OH)_2$, NH_2CHO, CH_3CHO, and C_2H_5OH, show compact emission (independent of excitation level),

whereas others show more extended emission (Manigand et al. 2020). This spatial differentiation seems to be related to the derived excitation temperature of the species ranging from above 90 K to 180 K with those having higher excitation temperatures showing more compact emission. Toward the other, lower luminosity, component of the system, IRAS 16293B, no significant spatial differentiation is resolved at 0.5-arcsec angular resolution. However, variations in excitation temperatures are also seen on smaller scales stretching over a somewhat larger range from about 100 to 300 K (Jørgensen et al. 2016) with a few species (e.g., CH_3OH, CH_3OCHO) showing evidence for an optically thick foreground layer with temperatures of about 100 K, with the bulk of the optically thin emission originating from molecules at the higher temperatures. A possible explanation for the spatial differentiation and variations in excitation temperatures may lie in the binding energies of the individual species in the ices causing this spatial stratification (Manigand et al. 2020), as also suggested in connection with gas-grain chemical modeling of hot cores (e.g., Garrod 2013).

5. LINKING THE PHYSICAL AND CHEMICAL EVOLUTION OF PROTOSTARS

Over the past decade significant work has been done on searching for and characterizing the properties of disks around embedded protostars in their Class 0 and I stages. In particular, with the advances in sensitivity and angular resolution by ALMA and other millimeterwave interferometers, it is found that Keplerian disks exist around a large number of Class I protostars (e.g., Harsono et al. 2014, Yen et al. 2015a, Artur de la Villarmois et al. 2019) and at least some Class 0 protostars (Tobin et al. 2012, Murillo et al. 2013, Lindberg et al. 2014, Yen et al. 2017), whereas counterexamples in which no signs of Keplerian rotation are seen down to ∼10 au scales certainly also exist (e.g., Yen et al. 2015b, Jacobsen et al. 2019).

These high-resolution observations have brought forward the close link between the physical structure and evolution of young stars and their disks and their astrochemistry. In particular, the youngest circumstellar disks serve as an interesting conduit between the COMs observed in the warm gas (Section 3.2) and the initial conditions for its later, protoplanetary, evolution. However, on the scales of the protostellar envelopes in which the temperatures increase above 100 K due to heating by the central protostar and complex organics sublimate from ices, the physics due to the presence of the disks becomes highly nontrivial (see also **Figure 1**). Also, the degree by which the chemistry may be altered, or even completely reset, as material is accreted to the disk, remains unclear. In this section, we discuss recent results concerning the link between the physical and chemical evolution of embedded protostars with particular focus on the formation of disks and accretion.

5.1. Chemical Changes in the Transitions from Envelopes to Disks

From a theoretical physical point of view, the formation of a circumstellar disk is thought to be associated with the presence of accretion shocks in which material enters the newly formed disk (e.g., Cassen & Moosman 1981, Neufeld & Hollenbach 1994). Recent calculations also suggest that shocks produced by accretion onto the protostellar surface itself may enhance the cosmic-ray ionization rate on large scales in more clustered environments compared to that of external sources, thereby potentially also affecting the chemical structure (Gaches & Offner 2018).

Based on *Spitzer Space Telescope* observations of water lines toward the Class 0 protostar NGC 1333-IRAS 4B, Watson et al. (2007) suggested that the water vapor had its origin in the warm and dense gas possibly related to an accretion shock due to infall from the protostellar envelope onto a very young disk. However, images of the IR lines from *Herschel* and *Spitzer* show that the

water line emission is in fact related to the outflow to the south (Herczeg et al. 2012). This is in contrast to narrow, i.e., nonshocked, line emission of the $H_2{}^{18}O$ isotopologue that peaks toward the embedded protostar itself (Jørgensen & van Dishoeck 2010b).

Using ALMA, Sakai et al. (2014) found kinematical evidence of a distinct component, the so-called centrifugal barrier, in a region of about 100 au separated from the Class 0 protostar L1527 and surrounding its Keplerian disk. Sakai et al. (2014) showed that sulfur monoxide (SO) and other sulfur-containing species were enhanced at this location and argued that this was a result of sublimation of grain mantles due to a weak accretion shock. Subsequent studies of other protostars show similar kinematical features, although in different molecular tracers (e.g., Oya et al. 2016, 2017; Sakai et al. 2016). In an ALMA survey of a sample of protostars from the Ophiuchus star-forming region, Artur de la Villarmois et al. (2018, 2019) detected warm ($E_{up} \approx 200$ K) SO_2 lines toward five of the more luminous sources. The lines were found to be wide and, in some cases, showed velocity gradients perpendicular to the outflow direction, which is a possible indication that the emission is related to shocks toward the surfaces of the emerging disks—although the compact nature of the emission made it impossible to rule out, for example, an outflow or jet origin.

Indications of accretion shocks at the envelope–disk interface have also been suggested for high-mass protostars. In high angular resolution ALMA observations of a massive protostar associated with the massive clump G328.2551–0.5321, Csengeri et al. (2018) found evidence for CH_3OH emission spots spatially offset from the central unresolved continuum emission associated with the protostar (see Section 4.3 and **Figure 6**). Based on the distinct kinematics of the CH_3OH emission compared with the outflow traced by lines of SiO and SO_2, Csengeri et al. argued that the CH_3OH peaks are associated with accretion shocks at the centrifugal barrier, whereas a transition of HC_3N in its first vibrationally excited state shows more compact emission, possibly tracing the properties of the accretion disks around more massive protostars.

However, significant work still needs to be done to establish an internally consistent picture of the different kinematical and chemical components of protostars as illustrated by different interpretations of similar observations of individual sources. For example, Oya et al. (2016) argued that CH_3OH and other COMs were present at the centrifugal barrier toward IRAS 16293A as a result of either a weak accretion shock or protostellar heating, in contrast to H_2CS that also traces the disk on smaller scales. By contrast, van 't Hoff et al. (2019) found that multiple spatially resolved H_2CS transitions were consistent with the temperature in a passively heated envelope down to small scales overlapping with the emission from some of the complex organics.

Another example is offered by the Class 0 protostar, L483, for which unsaturated carbon-chain species are present on large, single-dish, scales (e.g., Sakai et al. 2009; Agúndez et al. 2008, 2019), whereas saturated COMs are present on small, interferometric scales (Oya et al. 2017, Jacobsen et al. 2019). Based on the kinematical model of carbon monosulfide (CS) emission, Oya et al. (2017) argued that the centrifugal barrier in this source is at radii of 30–200 au with COM and SO emission possibly tracing an unresolved Keplerian disk within this. However, Jacobsen et al. (2019) demonstrated that the emission from CS and the COMs both show similar kinematical signatures consistent with material infalling under the conservation of angular momentum down to radii of 10–15 au rather than Keplerian rotation.

5.2. The Physical/Chemical Structure of Embedded Disks

For protostars with established Keplerian disks, other interesting questions arise concerning their physical structures: Does the distribution of molecules in the gas and ices in these disks reflect those around more evolved (T Tauri) stars in which significant freeze-out appears in the midplane,

or does the active accretion change the physical structures, for example by increasing the disk temperatures that are critical for the resulting chemistry? Through radiative transfer modeling of gas-phase lines observed with the SMA toward two Class I protostars with well-established disks, Brinch & Jørgensen (2013) found the former to be the case: Relatively simple models for T Tauri disks could be applied to those sources with simple chemistry dictated by the amount of shielding, in turn determining in what fraction of the disk CO is frozen out. A counterexample is offered by the disk around the more deeply embedded protostar L1527: By comparing ALMA data to detailed radiative transfer models, van 't Hoff et al. (2018b) showed that even in the midplane of this disk, the temperature is above 20 K out to radii of at least 75 au, thereby causing CO to be in the gas phase in the bulk of the disk.

The exact distribution and location of complex organics around Class I protostellar sources also remains puzzling. Toward the protostars in the ALMA Ophiuchus survey by Artur de la Villarmois et al. (2019), no significant emission from lines in the prominent CH_3OH 7_k–6_k branch was seen toward the locations of the protostars. These results demonstrate that the warm regions of the disk, where gas-phase CH_3OH can be present (or where weak shocks could act), must be relatively limited in extent and that the envelopes surrounding these disks must have relatively low column densities of material in their inner warm regions. In the standard picture of rotating collapse of a protostellar core and disk formation, the latter would be a natural consequence with the envelope density profile flattening out on small scales where the disk emerges. A simple prediction would consequently be that the presence of complex organics in the envelopes on small scales and the presence of extended Keplerian disks should be anticorrelated.

Recently, Lee et al. (2017, 2019a) presented an in-depth analysis of the HH 212 protostellar system in the L1630 cloud of Orion. The system shows a characteristic morphology with an edge-on dust lane with emission from COMs distributed parallel to the dust lane but offset above and below it. The complex organics show signs of a velocity gradient in the elongated direction, which is indicative of rotating motions (the region of the disk in which Keplerian motions would be present is only marginally resolved). These features led Lee et al. (2017) to suggest that these species are present in the atmosphere of the disk and formed either in the cold regions at large scales and sublimated at high temperatures in the disk atmospheres or, alternatively, through rapid gas-phase reactions there.

Another example of differentiation between dust continuum and line emission is seen toward the Class I protostar TMC1A. Through ALMA long-baseline observations of that source, Harsono et al. (2018) demonstrated that the emission of CO isotopologues (^{13}CO and $C^{18}O$) was clearly offset from the central location of the protostar and resolved dust continuum emission. Through detailed line radiative transfer modeling, Harsono et al. show that this differentiation in TMC1A can be best explained by the existence of large (millimeter-sized) grains causing the dust to become optically thick and thus blocking the emission of the gas lines. Due to the high column densities traced by ALMA in its long baseline configurations, some care must be taken when interpreting the spatial differentiation between species and dust emission on these scales due to the high continuum optical depth even in the absence of large grains such as those inferred by Harsono et al. (see Section 2.1.3).

5.3. Episodic Accretion and Snow Lines in Protostellar Envelopes

The emergence of disks around embedded protostars may also have profound implications on the overall physical evolution of the infalling material from the protostellar envelopes. If disks around the embedded protostars are comparable in mass with those around more evolved T Tauri stars

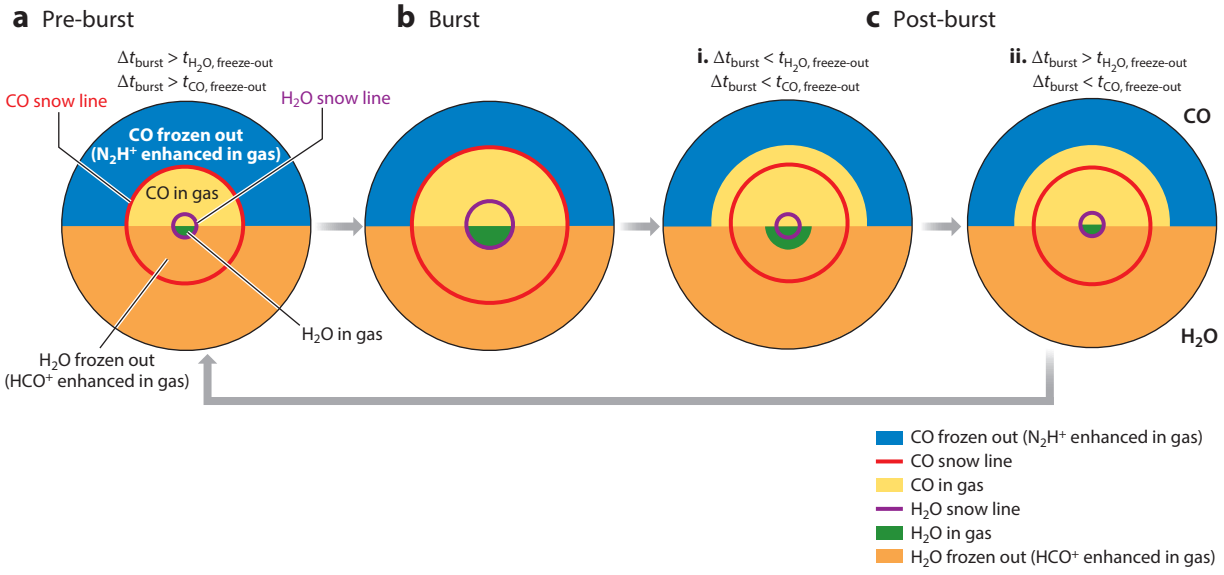

Figure 7

Changes of the chemical signatures of an embedded protostellar envelope before, during, and after a burst in accretion or temporal increase in luminosity. (*a*) Before the burst, molecules are frozen out on grains beyond the snow lines of the individual species (CO and H_2O illustrated at the *top* and *bottom*, respectively, as examples) and in the gas phase within these. Species destroyed through gas-phase chemical reactions with those species are enhanced in the regions where they are frozen out (e.g., N_2H^+ and HCO^+ enhanced where CO and H_2O, respectively, are frozen out). (*b*) During the burst, the luminosity of the protostar, and thus the temperatures in the envelope, increase. As a consequence the snow lines are shifted to larger radii, where the species are sublimated instantaneously. (*c*) In the quiescent phase after the burst, the snow lines shift inward again, but due to the density dependence of the freeze-out process, molecules remain in the gas phase for a longer period of time. The timescale for each species depends on the density of where its snow line is located. Eventually the freeze-out brings the chemistry down to its original state, again assuming that the time interval between bursts, Δt_{burst}, is longer than the molecular freeze-out timescales. For further background for this figure, see Jørgensen et al. (2013, 2015).

as is suggested by dust continuum observations (e.g., Jørgensen et al. 2009, Tychoniec et al. 2018), these disks may easily undergo periods of instability causing the accretion onto the central stars, and consequently their luminosities, to be nonsteady (episodic)—thereby also causing the temperatures in the ambient disk and envelope heated by the central protostar to vary. Observationally, there is photometric evidence, both statistically (see Audard et al. 2014 and Dunham et al. 2014 and references therein) and for individual protostars (e.g., Safron et al. 2015), that such luminosity variations indeed take place.

From a chemical point of view, temporal changes in the temperatures are naturally very important. For example, an (episodic) increase in luminosity for a given protostar will cause the regions where specific molecules sublimate from the surfaces of grains to become more extended compared to sources in a more quiescent phase of steady accretion (e.g., Lee 2007, Visser & Bergin 2012, Visser et al. 2015, Rab et al. 2017; see **Figure 7**). As the timescale for the subsequent freeze-out may be long (inversely proportional to the density) compared to the duration of such bursts, those extended regions of sublimated molecules may persist for significant periods of time even after the protostar has returned to its quiescent phase. Thus, observations of the molecular signatures of embedded protostars may provide an archeological view of their recent evolution. Episodic accretion events may also be reflected in the observed ice and dust features of the protostars. For example, the existence of pure CO_2 ices observed in the mid-IR spectra

of protostars is an indication that some thermal processing and subsequent freeze-out has taken place at some point during the preceding evolution (e.g., Ehrenfreund et al. 1997, Gerakines et al. 1999), possibly due to previous accretion bursts (e.g., Kim et al. 2012, Poteet et al. 2013). Taquet et al. (2016) demonstrated that the cyclic sublimation and freeze-out of the icy mantles could lead to the build-up of appreciable amounts of complex organic species in the inner envelopes of protostars.

Observationally, these suggestions can be tested by measuring the extents of primary species directly sublimating from grains or secondary species either produced or destroyed subsequently in the gas phase (**Figure 7**). Studies of the images of the $C^{18}O$ emission toward protostars observed with the SMA (Jørgensen et al. 2015, Frimann et al. 2017) show evidence for emission extending beyond the predictions based on the current luminosities for 20–50% of the sources. Given that the timescale for $C^{18}O$ to freeze out is of order 10^4 years at the densities at which it is found in the gas phase for these protostars, the statistics suggest that each protostar typically undergoes an accretion burst once every $2–5 \times 10^4$ years, resulting in an increase in its luminosity by 1–2 orders of magnitude. A comparison to numerical predictions of large-scale MHD simulations demonstrates that these results are robust even when the possible complex geometry of the sources is taken into account (Frimann et al. 2016). An alternative to targeting the CO isotopologues is to look for the absence of N_2H^+ emission toward the center of the protostar where CO sublimates. Spatially resolved images of the emission from N_2H^+ and CO show these species to be anticorrelated. For example, Anderl et al. (2016) presented observations and modeling of N_2H^+ toward four nonbursting protostars from the sample studied in $C^{18}O$ by Jørgensen et al. (2015) and show that the N_2H^+ structure indeed was consistent with that seen in $C^{18}O$, as well as the current luminosities of the sources. Hsieh et al. (2018) used ALMA to observe seven very low-luminosity protostars (VeLLOs or very low luminosity objects) in $C^{18}O$ and N_2H^+ and found that for five of those sources, the $C^{18}O$ emission and related N_2H^+ suppression implied recent accretion bursts with a time interval between bursts of $1.2–1.4 \times 10^4$ years.

Complementary constraints to those from CO and N_2H^+ observations can be obtained by observing species that sublimate at different radii due to their different binding energies in the ices. Because of the decrease in density with increasing radii in the protostellar envelopes, this would cause the freeze-out timescale for such species to differ from those of CO, thus providing complementary information concerning the frequencies and magnitudes of the bursts. A particularly interesting example is that of H_2O, which sublimates at much smaller scales of the protostellar envelope where the temperature exceeds 90–100 K, compared to the 20–30 K of CO, and consequently freezes out much more quickly again. Water is difficult to image using millimeter wavelength interferometers due to Earth's atmosphere, but species such as HCO^+ are suppressed by the presence of H_2O, in a similar way as N_2H^+ is by CO, and can thus be used as indirect tracers (Visser et al. 2015, and **Figure 7**). Indeed, images of the $H_2^{18}O$ and $H^{13}CO^+$ isotopologues of these species toward the Class 0 protostars NGC 1333-IRAS 2A (van 't Hoff et al. 2018a) and IRAS 15398-3359 (Jørgensen et al. 2013, Bjerkeli et al. 2016a) show similar anticorrelations to those of CO and N_2H^+ but on much smaller scales. The extent of this HCO^+ suppression toward IRAS 15398-3359 (Jørgensen et al. 2013) implies that the protostar has undergone a recent burst but only within the previous 100–1,000 years. High angular resolution images of the CO outflow from this source show the presence of bullet-like structures, also supporting the interpretation of ejection events on ∼100-year timescales (Bjerkeli et al. 2016b). Another example is the FU Orionis object V883 Ori for which an increased luminosity moved the water snowline outward and led to large column densities of methanol and other COMs over extended regions where they are observable with ALMA (van 't Hoff et al. 2018c, Lee et al. 2019b).

Hsieh et al. (2019) performed a statistical survey of N_2H^+ and HCO^+ using ALMA toward 39 Class 0 and I protostars from the Perseus molecular cloud. Almost all sources in their sample show evidence for postburst signatures in N_2H^+, whereas the number of sources with postburst signatures in HCO^+ decreases from the Class 0 to I stages. These differences suggest that the time intervals between bursts increase from 2,400 years in the Class 0 stage to 8,000 years in the Class I stage. An explanation for this evolution could be that the accretion bursts are results of instabilities in disks that are more likely to occur in the earliest protostellar stages.

5.4. Summary

The above discussions raise a number of outstanding questions concerning the physical and chemical structure of embedded disks and their formation and evolution. Are the pictures of accretion shocks and episodic accretion generally applicable? To what degree do these cause the chemistry to be reset or lead to differing chemistries with new molecules formed? How are COMs distributed around embedded protostars, and do they point to one physical origin, or perhaps several different ones connected to those shown in **Figure 1**? What role does grain growth play in the chemical evolution as well as the interpretation of line emission and chemistry on small scales? These discussions are still suffering from a lack of unbiased data sets that are comparable in terms of the observed molecular line tracers. The obvious next step will therefore be to expand the observed number of sources and species systematically, and establish generally applicable models that can account for the differences between low- and high-mass protostars and, importantly, make predictive statements.

6. FRACTIONATION

One of the important tools to study the physics and chemistry of the ISM is to target less abundant isotopologues of specific species (see the sidebar titled Isotopologues and Isotopomers). This may be a useful way of finding transitions that, though optically thick for the main isotopologue, may be optically thin for the rarer isotopologue due to its lower column density. However, from an astrochemical point of view, it is also well established that for many molecular species in the ISM, the isotope ratios (e.g., D/H, $^{12}C/^{13}C$, or $^{14}N/^{15}N$) measured as column density ratios between their isotopologues differ significantly from the elemental abundances representative for the local conditions in their ambient ISM. These variations, referred to as isotopic fractionation, can be either enhancements or depletions of the rarer isotopologues compared to the local ISM isotopic ratio and range numerically from a factor of a few differences for the heavier elements, such as carbon and nitrogen, to enhancements of several orders of magnitude for deuterium. In the Solar System, significant variations are also seen in the isotopic compositions in different

ISOTOPOLOGUES AND ISOTOPOMERS

Isotopologues refer to molecules that only differ in their isotopic composition. Isotopologues can have one or more atoms substituted by isotopes, occasionally referred to as singly, doubly, etc., substituted variants. Isotopomers, or isotopic isomers, are species that consist of the same number of each isotopic atom, but the positions of those atoms within the molecule differ. As examples, CH_2DOH, CH_3OD, $^{13}CH_3OH$, and $CH_3^{18}OH$ are singly substituted isotopologues of methanol, CH_3OH. Of these, CH_2DOH and CH_3OD are isotopomers, where the D-isotope is substituted on either the CH_3 or OH functional group.

bodies and materials. As these variations are thought to reflect processes that took place during the earliest stages of the Solar System, a detailed understanding of the different physical and chemical processes behind isotopic fractionation may shed light on its origin and relation to star and planet formation as we observe it now.

A range of processes can lead to isotopic fractionation in the ISM. For common species such as CO and N_2, the high abundance of the main isotopologues, and thus opacity at the frequencies of their transitions, causes these species to be self-shielded against photodissociation, whereas their rarer isotopologues may be photodissociated over larger columns. As a result of this isotope-selective photodissociation [see, e.g., Visser et al. (2009) for the case of CO and Heays et al. (2014) for N_2], the molecular carrier becomes depleted in the rarer isotopic variant as the depth or extinction increases (^{12}CO becomes more abundant than ^{13}CO compared to the ^{12}C/^{13}C ratio, $^{14}N_2$ more abundant than $^{15}N^{14}N$ compared to the ^{14}N/^{15}N ratio etc.) while the atomic gas becomes enriched in the rarer isotope (^{13}C, ^{15}N, etc.). Depending on the exact chemical networks, both the molecular and atomic isotopic signatures may be carried over to other gaseous species and possibly solids (e.g., Lyons & Young 2005, Furuya & Aikawa 2018). The efficiency of these processes naturally depends on the strength and spectral shape of the incoming radiation as well as physical conditions in the environment, e.g., the distribution of material and shielding by grains.

Deeper in the cloud, chemical fractionation may play a more prominent role. A classical example is the balance between H and D through the isotope exchange reaction:

$$H_3^+ + HD \quad \leftrightarrow \quad H_2D^+ + H_2. \qquad 1.$$

At the low temperatures of prestellar cores, the exothermicity of this reaction causes the deuterium of HD to be driven toward H_2D^+, which thus becomes increasingly abundant relative to H_3^+. As H_3^+ is one of the key ingredients for many gas-phase chemical networks in the ISM, its enhanced deuteration can then be carried to a number of other common species, such as HCO^+ and N_2H^+ enhancing the abundance of their deuterated isotopologues. The above reaction also has an important role in determining the D/H ratios for species formed on grain surfaces: The main source of atomic H or D in star-forming regions is through dissociative recombination of H_3^+ or H_2D^+ with electrons. Thus, the overabundance of H_2D^+ leads to an enhanced atomic D/H ratio in the gas at low temperatures, which can be transferred to molecules formed on grains through hydrogenation of neutral species (Tielens 1983). The effectiveness of these deuteration processes depends on a number of factors, including the temperature, the freeze-out of species such as CO, which acts as the main destroyer of H_3^+ and H_2D^+, and the ortho-to-para ratios of the species in Equation 1 (e.g., Sipilä et al. 2015).

In this section, we discuss the origin of isotopic fractionation as it occurs in connection to the process of star formation. The intent is not to provide a comprehensive review of all observational and modeling efforts. Rather, we highlight a few key points with particular emphasis on how measurements of the relative abundances of different isotopologues can be used to trace the link between complex species and water in star-forming environments and the Solar System.

6.1. Water

Perhaps, the most well-known discussion of fractionation in regions of star formation and the link to the Solar System concerns the origin of Earth's water and its deuterium isotopic composition compared to Solar System bodies and star-forming regions. It has long been known that the D/H ratio in Earth's oceans of 1.5×10^{-4} (e.g., Robert et al. 2000) is enhanced compared to the cosmic D/H ratio of 1.5–2.0 $\times 10^{-5}$ (e.g., Linsky 2003, Prodanović et al. 2010). Furthermore, a number of other Solar System bodies including comets (e.g., Lis et al. 2013) and meteorites (e.g., Alexander

et al. 2012) are also known to show enhanced D/H ratios. Although a lot of emphasis has been put on understanding the delivery of water to Earth through comparisons of the D/H ratios between these bodies, e.g., whether water was brought to Earth through cometary or meteoritic impacts, another relevant question from a star-formation astrochemical point of view is when water was formed and how much processing occurred before it ended up as ices in the protoplanetary disk. Through detailed models of the water deuterium chemistry, Cleeves et al. (2014) and Furuya et al. (2017) found that the formation of deuterated water is inefficient in the disk itself, but rather inherited without significant alteration from the earlier prestellar stages. These results highlight the importance of the prestellar chemistry for the origin of water in both our own Solar System and other planetary systems.

Knowledge about the water deuteration in star-forming regions comes largely from gas-phase observations at far-IR and (sub)millimeter wavelengths. In general, the column densities of water ice are large toward pre- and protostellar cores, and the ice solid-state features can readily be studied at IR wavelengths. However, the corresponding solid-state features of deuterated water, HDO, are difficult to disentangle due to sensitivity and overlap with more prominent species (e.g., Dartois et al. 2003) and only tentative detections have been reported toward solar-type protostars (Aikawa et al. 2012).

With, in particular, its HIFI (Heterodyne Instrument for the Far Infrared) instrument, *Herschel* provided significant insight into the distribution of gaseous water around solar-type protostars. Those observations demonstrated that small amounts of water are present in the gas phase at large scales of protostellar envelopes (Coutens et al. 2012, Mottram et al. 2013) as well as cold prestellar cores (Caselli et al. 2010), a result of cosmic rays causing the water to photodesorb off the grains (Caselli et al. 2012). The abundance of water in the gas phase remains low, but still the column densities are high enough that HDO emission from the same regions could be estimated for a few sources. In those regions, the HDO/H_2O ratio is determined by gas-phase chemistry at low temperatures and was found to range from $\sim$1% to 20% (Liu et al. 2011; Coutens et al. 2012, 2013).

Deriving the D/H ratios of water ices sublimating in the warm regions close to the central protostar using single-dish and *Herschel* measurements is more problematic: These regions are heavily diluted in the large beams of such observations, and the interpretation therefore heavily depends on radiative transfer models of the emission, which in turn are complicated due to the separation of the multiple (unconstrained) physical components within the beam and the fact that both the dust and some prominent lines become optically thick on small scales (e.g., Visser et al. 2013). Alternatively, interferometric studies of lines of less abundant isotopologues make it possible to zoom in and constrain the column densities of water on comparable scales in which the emitting regions are relatively homogeneous in terms of their physics and the densities high enough that LTE is a reasonable approximation (see discussions in Taquet et al. 2013, Persson et al. 2014). In this manner, estimates of the HDO/H_2O ratios have been derived for the typical Class 0 hot corinos with values of order 0.1% (e.g., Jørgensen & van Dishoeck 2010a; Persson et al. 2013, 2014; Taquet et al. 2013), i.e., more than an order of magnitude below those found on larger scales and more in line with the highest numbers found for Oort family comets in our own Solar System.

The differences between the D/H ratios in the cold gas in the outer envelope and in the warm gas on small scales can be successfully modeled in different manners. The increased D/H ratio on large scales is caused by either photodesorption, predominantly acting on the outermost layers of ice mantles that are formed latest and therefore most deuterium rich (Taquet et al. 2014), or continued gas-phase deuteration of water once desorbed (Furuya et al. 2016).

The same models must also explain measured differences in the deuteration between the singly and doubly deuterated variants of water, i.e., the HDO/H_2O and D_2O/HDO abundance ratios specifically. Statistically, the former ratio should be four times higher than the latter, because there are two indistinguishable variants of singly deuterated water depending on which H atom is substituted. However, direct interferometric measurements show that the D_2O/HDO ratio is in fact higher than the HDO/H_2O ratio by a factor of 7 (Coutens et al. 2014)—i.e., D_2O is more than an order of magnitude more abundant than HDO with respect to what should be expected from the HDO/H_2O ratio and the statistics mentioned above. In the models by Furuya et al. (2016), the higher D_2O/HDO ratio can be explained if water ice forms throughout the evolution of the dense prestellar cores, from the earliest more tenuous stages in which the D/H ratio is low to the later stages in which CO freezes out and a drop in the ortho-to-para ratio of H_2 causes the deuteration to be more efficient. In this scenario, the bulk of the (nondeuterated) water forms early in this evolution, whereas the deuterated species (HDO and D_2O) are formed in the dense stages and their relative abundances thus reflect the higher D/H ratios there.

Although studies of water's D/H ratios show interesting potential for studies of its formation under different conditions, it should be cautioned that the samples are still relatively small. A few studies have started addressing, e.g., the temporal and environmental variations. For example, toward the Class I protostar SVS13b, Codella et al. (2016) derive limits to the HDO/H_2O comparable with that of the Class 0 protostars, which again could be taken as an argument in favor of the water formation and deuteration during the prestellar phases and little processing happening during the evolution of the protostars themselves. An example of the potential environmental dependence is seen in recent measurements by Jensen et al. (2019) of the HDO/H_2O ratios toward three protostars located in more isolated cores (**Figure 8**). The HDO/H_2O ratios for those sources are remarkably consistent and higher by factors of 2–4 compared to those for the classical hot corinos located in more clustered regions. These differences could reflect the physics in the

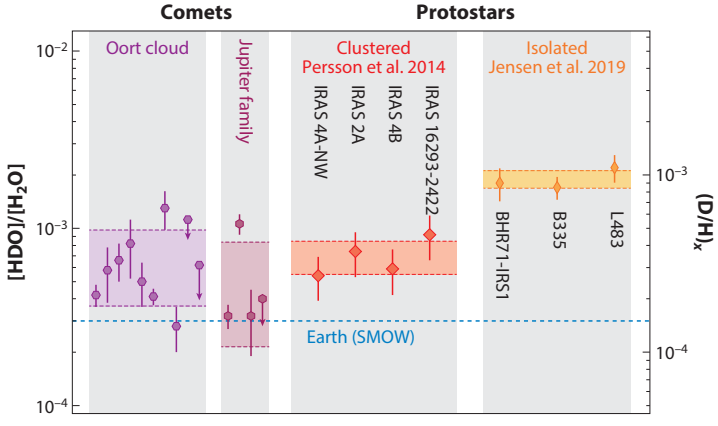

Figure 8

Measurements of the HDO/H_2O abundance (*left axis*) and D/H ratio corrected for statistics (i.e., when taking into account the number of equivalent hydrogen atoms; *right axis*) toward Oort cloud and Jupiter family comets as well as protostars formed in clustered and more isolated regions. The two groups of protostars show a difference in the HDO/H_2O ratios by a factor of 2–4 with the ratios for the protostars from the more clustered regions closer to those of the comets. These differences may reflect the conditions in the parental environments of the protostars and provide a diagnostic for the environments in which the Sun was formed. Figure based on Jensen et al. (2019) and references therein. Abbreviation: SMOW, standard mean ocean water.

environment from which they arise, with the more isolated cores forming in colder environments and/or evolving more slowly through those. However, to fully disentangle these effects, it is clearly necessary to expand the samples of well-studied sources to other regions and compare with other tracers of the (temporal) protostellar chemical evolution.

6.2. Complex Organics

The characterization of the isotopic ratios of COMs also provides important insight into the astrochemistry in star-forming regions. The good relative calibration across the ALMA bands, and the number of transitions any COM isotopologue typically shows in these regions, makes it possible to derive the relative abundances and thus levels of fractionation with high accuracy if the isotopologues coexist in the high-density environment in which LTE applies.

The first interstellar detections of deuterated methanol were obtained toward the Orion KL region with the IRAM 30-m telescope for both CH_3OD and CH_2DOH (Mauersberger et al. 1988, Jacq et al. 1993). The deuterium fractionation of methanol as traced more recently with PdBI and *Herschel* is 0.5–0.6% toward the compact ridge and lower than 0.4% toward the hot core (Peng et al. 2012, Neill et al. 2013). Deuterated methyl formate was also first detected in the ISM toward Orion KL with the 30-m telescope, CH_3OCDO only tentatively but CH_2DOCHO robustly, and both with a deuterium fractionation of ∼4% with some variations across the region (Margulès et al. 2010, Coudert et al. 2013). The different deuteration levels of methanol and methyl formate may indicate that the former was formed at earlier stages than the latter.

A systematic study of the deuteration of COMs in Sgr B2(N2) was performed with the EMoCA survey (Belloche et al. 2016). The low level of deuteration found for a few COMs in Sgr B2(N2) compared to Orion KL and other high-mass protostellar objects surveyed in methanol by Fontani et al. (2015) was interpreted as resulting from either the higher prestellar-phase temperatures that seem to characterize the Galactic Center region or a lower elemental abundance of deuterium itself in the Galactic Center region due to stellar processing, as was argued in the past on the basis of measurements performed with smaller molecules on larger scales, albeit with large uncertainties (Jacq et al. 1999, Lubowich et al. 2000, Polehampton et al. 2002). Measurements toward the hot cores NGC 6334I (Bøgelund et al. 2018) and NGC 7538-IRS1 (Ospina-Zamudio et al. 2019), both located in the Galactic disk, found low values similar to Sgr B2(N2), which supports the temperature interpretation for Sgr B2 rather than that of the astration.

Compared with the high-mass star-forming regions, the degree of deuteration is much higher toward low-mass protostars such as IRAS 16293-2422 as witnessed by early measurements (van Dishoeck et al. 1995) as well as detections of doubly and triply deuterated variants of species such as CH_3OH (e.g., Parise et al. 2002, 2004) using single-dish telescopes. Toward the two main components of this source, the PILS survey has provided systematic inventories of the D/H ratios as well as some estimates of $^{12}C/^{13}C$ ratios for COMs (Coutens et al. 2016; Jørgensen et al. 2016, 2018; Calcutt et al. 2018b; Manigand et al. 2020). For some species the D/H ratios can be as high as 5–8%, which translate to the abundance of the deuterated isotopologues relative to the main isotopologues in some cases being as high as 20% due to statistics (see also discussion of water above). In fact, in the context of PILS, most deuterated isotopologues of two-carbon-containing COMs for which spectroscopy is available have been identified.

Interestingly, some variations are seen in the deuteration between different species toward the B component of IRAS 16293-2422. Toward that source a range of the two carbon-atom containing species including CH_2OHCHO (Jørgensen et al. 2016), CH_3CHO, CH_3OCHO, CH_3OCH_3, and C_2H_5OH (Jørgensen et al. 2018) all show ratios of 4–8%, whereas many of the smaller/simpler molecules, H_2CO (Persson et al. 2018), CH_3OH (Jørgensen et al. 2018), CH_3CN (Calcutt et al.

2018b), and the S-bearing species (Drozdovskaya et al. 2018), show lower ratios of ≈2%. Toward the other source, IRAS 16293A, the deuteration is similarly high for some species, but because of larger uncertainties no clear trend is discernible (Manigand et al. 2020). One possible explanation for this heterogeneity observed toward IRAS 16293B, and possibly also causing the differences between CH_3OH and CH_3OCHO toward Orion mentioned earlier, could be that the former group of species are formed later in the evolution of the protostellar core and inherit the D/H ratio then.

The $^{12}C/^{13}C$ ratios may also carry information. The spectral surveys performed toward Sgr B2(N) led to the determination of the $^{12}C/^{13}C$ isotopic ratio for a number of COMs. The EMoCA survey toward Sgr B2(N2) yields values of 20–21 for CH_3CN, C_2H_3CN, and HC_3N (Belloche et al. 2016) and 25–27 for CH_3OH, C_2H_5OH, and NH_2CHO (Müller et al. 2016a, Belloche et al. 2017), with uncertainties likely not higher than 10–15%. A ratio of 32 was derived from the singly ^{13}C-substituted isotopologues of C_2H_5CN, which is surprisingly high compared to the other cyanides, all the more so as the ratio derived from the singly and doubly ^{13}C-substituted isotopologues of C_2H_5CN is 26 (Margulès et al. 2016). The origin of this difference is still unclear. $^{12}C/^{13}C$ ratios were also derived from H_2CS, CH_3CCH, NH_2CHO, and C_2H_5CN toward Sgr B2(N) by Halfen et al. (2017) with their single-dish ARO survey. They obtained values ranging from 15 to 33 with uncertainties on the order of 30%, with an average value of 24 ± 9, which is consistent with the range of values derived from EMoCA. In IRAS 16293B, some indications were seen for differences in the $^{12}C/^{13}C$ ratio for a few of the species with higher D/H ratios, which, again, may reflect fractionation triggered by far-UV irradiation by the embedded protostar (Jørgensen et al. 2018).

Other important information about the formation of these organics may come from possible differences in the isotope ratios for different functional groups in individual COMs. Favre et al. (2014) studied the two ^{13}C isotopologues of methyl formate in Orion KL with ALMA and found no significant fractionation difference between the two variants. A similar conclusion was reached based on the EMoCA measurements of the $^{12}C/^{13}C$ ratios mentioned above. Toward IRAS 16293B, most of the complex organics do not show variations in their D/H ratios after accounting for the statistics when there are multiple hydrogen atoms (Jørgensen et al. 2016, 2018). This again suggests a homogeneous time of formation during the cold phase for each individual species at which point the D/H ratio is inherited, whereas exchange reactions later in the warm gas play a smaller role. There is one exception to this trend, namely CH_3CHO, for which the CHO-group shows a higher D/H ratio than the CH_3-group when corrected for statistics (Coudert et al. 2019, Manigand et al. 2020). Whether the D/H ratio for this species could be influenced by other (e.g., gas-phase) processes remains an open question.

It has been suggested that the CH_2DOH/CH_3OD ratio could vary between regions of low- and high-mass star formation (e.g., Ospina-Zamudio et al. 2019, and references therein), ranging from about unity toward Orion (or even lower toward NGC 6334I; see Bøgelund et al. 2018), over ratios of close to the statistical value of three toward high-mass protostars, to much higher ratios claimed toward low-mass star-forming regions. However, there are known issues with the predicted line intensities of CH_2DOH that may have caused the column density estimates to be off in some cases. Also, in particular, the higher ratios for low-mass sources have suffered from problems due to extended emission seen in single-dish beams as well as optical thickness of a range of the brighter CH_2DOH transitions. Recent estimates for the warm gas toward solar-type protostars are consistent with the statistical ratios (Jørgensen et al. 2018, Taquet et al. 2019). Consequently, though the estimates toward Orion indicate a CH_2DOH/CH_3OD ratio below the statistical value, which may reflect the physical structure of the region, the conclusion that there is a

dichotomy between low- and high-mass star-forming regions in terms of the CH_2DOH/CH_3OD ratios is not robust at this point.

A final puzzle is posed by the detections of doubly deuterated variants of a range of species on small scales toward IRAS 16293B, including H_2CO (Persson et al. 2018), CH_3CN (Calcutt et al. 2018b), and CH_3OCHO (Manigand et al. 2019). As seen for water, the D/H ratios derived from the ratios of the column densities for the doubly and singly deuterated isotopologues are significantly higher by factors of 5–10 than those derived from the singly and nondeuterated isotopologues once corrected for statistics. However, if these species are all formed in the later stages through hydrogenation of CO-rich ices, this difference can, in contrast to water, not be attributed to differences in formation times between the various isotopologues. Alternative mechanisms could be abstraction and substitution reactions, but as noted above those need to be equally efficient for different functional groups of a given molecule (see discussion in Manigand et al. 2019).

7. ORIGIN AND EVOLUTION OF CHEMICAL COMPLEXITY

As described throughout this review, one of the ultimate goals of astrochemistry is to understand the degree of chemical complexity that can arise before and during the star-formation process and how much, if any, of this complexity may be inherited by emerging (proto)planetary systems in general. With the wide diversity of environments in which COMs are now detected (Sections 3 and 4) and their intricate link to the physical evolution of individual sources (Section 5), a key question is to what degree the chemistry varies. With the systematic inventories of molecular species becoming available for objects in different evolutionary stages and environments, some clues to answering these questions may be obtained by comparing them. Held together with detailed comparison of the isotopic compositions (Section 6), the hope is that such measurements will help us to place the origin of our own Solar System and its chemistry in a more general star- (and planet-)formation context. In this section, we pick up this thread in a discussion of similarities and differences among measured abundances of complex organic molecules toward different types of environments related to star formation, recent cometary values, and predictions from chemical models.

7.1. Similarities and Differences Between IRAS 16293B, Sgr B2(N2), and Comet 67P/C-G

An example of such a comparison between the PILS IRAS 16293B results and measurements toward Comet 67P/C-G obtained from the ROSINA (Rosetta Orbiter Spectrometer for Ion and Neutral Analysis) instrument on *Rosetta* is presented by Drozdovskaya et al. (2019). Their results show a correlation between the protostellar and cometary measurements of the abundances of the CHO-, N-, and S-bearing species when estimated relative to CH_3OH, CH_3CN, and CH_3SH, although with some scatter. For the CHO- and N-bearing species the cometary relative abundances are slightly enhanced compared to the protostellar abundances. Drozdovskaya et al. (2019) concluded that the volatiles present at the earliest stages of the protostellar evolution are inherited by the cometary bodies, but also that some additional degree of processing could have occurred during the protoplanetary disk stage leading to further production of more complex species.

Obviously, a relevant question in this comparison is how representative IRAS 16293B is for the environment of the protosun and, more generally, how much variation is seen between different star-forming regions. To start addressing these questions, **Figure 9** compares the abundances toward IRAS 16293B from PILS with those toward Sgr B2(N2) from EMoCA (**Figure 9*a***), with the same species from the *Rosetta* values for Comet 67P/C-G (**Figure 9*b***), as well as results from

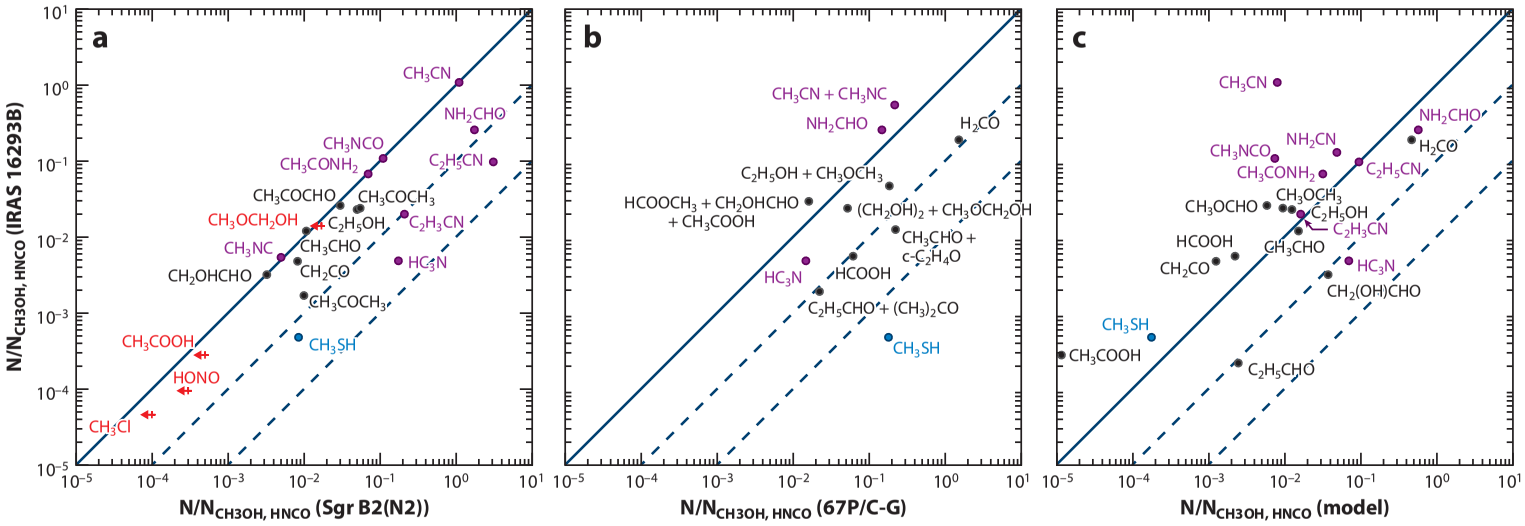

Figure 9

Comparison between the abundances of IRAS 16293B from the PILS survey to those toward (*a*) Sgr B2(N2) from the EMoCA survey, (*b*) a subset of those measured for Comet 67P/C-G from *Rosetta*, and (*c*) in models. The abundances are measured relative to HNCO for the N-bearing species (*purple data points*) and CH_3OH for the O-bearing species (*black data points* and *upper limits* shown in *red*) and CH_3SH (*blue data points*). The lines indicate one-to-one abundances (*solid line*) and factors of 10 and 100 enhancement in Sgr B2(N2), Comet 67P/C-G, or the models compared with IRAS 16293B (*dashed lines*). A list of the molecular abundances and references are provided in **Table 2**.

Table 2 Abundances relative to CH_3OH used in Figure 9 from measurements toward IRAS 16293B, Sgr B2(N2), and Comet 67P/C-G as well as those predicted by models

Species	IRAS 16293B[a] (PILS) (%)	Sgr B2(N2)[b] (EMoCA) (%)	Model predictions[c] (%)	Comet 67P/C-G[d] (%)
CH_3OH	100	100	100	100
H_2CO	19	NA	48	150
C_2H_5OH	2.3	5.0	1.3	19[e]
CH_3OCH_3	2.4	5.5	0.96	
CH_3OCHO	2.6	3.0	0.59	1.6[e]
CH_2OHCHO	0.34	0.33*	3.8	
CH_3COOH	0.028	<0.05*	0.0012	
CH_3CHO	1.2	1.1	1.5	22[e]
c-C_2H_4O	0.054	NA	NA	
CH_3OCH_2OH	1.4	<1.7*	0.44	5.2[e]
$(CH_2OH)_2$	0.99[f]	NA	NA	
CH_3COCH_3	0.17	1.0	NA	2.2[e]
C_2H_5CHO	0.022	NA	NA	
NH_2CHO	0.10	8.8	2.0	1.9
CH_3CN	0.40	5.5	0.028	2.8[e]
CH_3NC	0.0020	0.025	NA	
HNCO	0.37	5.0	3.4	13
HC_3N	0.0018	0.88	0.24	0.19
CH_3SH	0.048	0.85	0.018	18
CH_3NCO	0.040	0.55	0.026	NA
C_2H_5CN	0.036	16	0.33	NA
C_2H_3CN	0.0074	1.1	0.056	NA
CH_3CONH_2	0.025	0.35	0.11	NA
HONO	0.0090	<0.030*	NA	NA
CH_2CO	0.48	0.83*	0.13	NA
HCOOH	0.56	NA	0.23	6.2

Abbreviations: EMoCA, Exploring Molecular Complexity with ALMA; NA, not available; PILS, Protostellar Interferometric Line Survey; ROSINA, Rosetta Orbiter Spectrometer for Ion and Neutral Analysis.

[a]Measurements toward IRAS 16293B in connection with the PILS program (Jørgensen et al. 2016, 2018; Coutens et al. 2016, 2019; Lykke et al. 2017; Calcutt et al. 2018a,b; Ligterink et al. 2017; Drozdovskaya et al. 2018; Persson et al. 2018; Manigand et al. 2020; see also the summary by Drozdovskaya et al. 2019).

[b]Measurements toward Sgr B2(N2) in connection with the EMoCA program (Belloche et al. 2016, 2017; Müller et al. 2016a; Bonfand et al. 2019; Ordu et al. 2019; Willis et al. 2020). New measurements presented here for the first time (Belloche, private communication) are indicated with an "∗".

[c]Results from the MAGICKAL simulations presented by Müller et al. (2016a) and Belloche et al. (2017).

[d]Measurements from the ROSINA instrument presented by Drozdovskaya et al. (2019).

[e]Species indistinguishable in the ROSINA spectrometer measurements of Comet 67P/C-G.

[f]Refers to total abundance of the two lowest-state conformers, *aGg′* and *gGg′*, of ethylene glycol, $(CH_2OH)_2$.

the MAGICKAL simulations presented by Müller et al. (2016a) and Belloche et al. (2017) intended to reproduce the chemistry in Sgr B2(N2) (**Figure 9*c***). The full list of abundances and references are provided in **Table 2**. For the oxygen-bearing species and CH_3SH, we use CH_3OH as a reference species, and for the nitrogen-bearing species, we use HNCO. This choice of HNCO differs from Drozdovskaya et al. (2019), who normalized the nitrogen-bearing species relative to CH_3CN.

For the observed data sets this is not significant, as the HNCO/CH_3CN ratios are identical toward IRAS 16293B and Sgr B2(N2). However, in the models the CH_3CN abundance is significantly lower (see below), whereas adopting HNCO makes for a more direct comparison with the observations.

The most striking takeaway from **Figure 9** is the excellent correlation between the abundances measured toward IRAS 16293B and Sgr B2(N2) directly demonstrating that CH_3OH and HNCO (or CH_3CN) serve as good proxies for the groups of O- and N-bearing species toward IRAS 16293B and Sgr B2(N2). It is important to note that the abundances of HNCO relative to CH_3OH differ significantly. Relative to IRAS 16293B the HNCO/CH_3OH ratio is close to a factor of 14 higher toward Sgr B2(N2), a factor of 35 higher toward Comet 67P/C-G, and a factor of 9 higher in the models. These differences between the observed HNCO/CH_3OH ratios, and implicitly the difference between the O- and N-bearing species, may reflect an underlying chemical differentiation similar to those discussed in Section 4.3, e.g., because the groups of species trace different physical components toward the sources.

Figure 9 also indicates some other immediate trends. In terms of the overall variations, Sgr B2(N2) and IRAS 16293B are more similar to each other than to Comet 67P/C-G or to the hot core models. In fact, though the hot core models were set up to simulate the chemistry of Sgr B2(N2), they are actually in slightly better overall agreement with the abundances observed toward IRAS 16293B once the differences between the O- and N-bearing species are taken out through the normalizations with CH_3OH and HNCO. Specifically, the abundances are in general slightly lower in the models compared to IRAS 16293B, whereas the abundances toward Sgr B2(N2), with very few exceptions, are slightly higher than those toward IRAS 16293B, although only in a few cases by more than an order of magnitude.

Aside from NH_2CHO and the three nitrile group-bearing species, HC_3N, C_2H_3CN, and C_2H_5CN, the N-bearing species agree well between Sgr B2(N2) and IRAS 16293B. The fact that the C_2H_XCN species are similarly elevated toward Sgr B2(N2) over IRAS 16293B perhaps indicates that all three of these species are behaving in concert through some shared chemistry or common dependence on physical conditions. In the case of C_2H_3CN and C_2H_5CN, their similar behavior across sources may be at least partially explained by the chemical models, which suggest that gas-phase C_2H_3CN is a direct (and major) product of the destruction of gas-phase C_2H_5CN (see Garrod et al. 2017). Several competing theories have been offered as to the production mechanism for NH_2CHO in hot cores/corinos (see Section 2.3), including both gas and grain-surface processes. If indeed all of those suggested processes were operative, rather than one single, dominant process, then discrepancies between sources should perhaps be expected if not easily explained.

In the chemical models (**Figure 9*c***), abundances of most N-bearing species are lower than values from the observations and cometary measurements. It is possible that some of this general discrepancy relates to the use of a ratio against HNCO, if this molecule is not well reproduced by the models. However, the modeled abundance of CH_3CN is especially divergent from the observed value, falling as many as two orders of magnitude short. The models with which we compare here suggest that much of the gas-phase CH_3CN is formed through gas-phase chemistry at high temperatures and densities, although the dominance of this process would require a sufficient time period under such conditions. Other recent models (Bonfand et al. 2019) that use an alternative, and more detailed, physical description in conjunction with an updated binding energy for CH_3CN indicate a grain-surface origin for this molecule. The abundance of CH_3CN may therefore be especially sensitive to physical conditions and evolutionary timescales in individual sources, thus requiring a more accurate physical treatment in the chemical models to determine the origins of this molecule. Deeper integration of gas-grain chemical modeling treatments with

magnetohydrodynamical simulations of the star-formation process would be of great benefit to distinguishing between formation mechanisms for key molecules such as this, especially in the case where observations and models diverge by more than an order of magnitude.

The O-bearing species are even more closely correlated between IRAS 16293B and Sgr B2(N2) than the N-bearing species with, in particular, a number of the CHO species in almost 1-to-1 agreement. Comparing the O- and N-bearing species between IRAS 16293B and Comet 67P/C-G, the opposite is the case, with better agreement for the N-bearing species, whereas the O-bearing species are somewhat more abundant toward the comet as also noted by Drozdovskaya et al. (2019). The models reproduce the column densities for the O-bearing species within about an order of magnitude but with larger scatter compared to the observational data sets. Overall, CH_3SH does not show any systematic trends, but a comparison to CH_3OH is perhaps not the most obvious for that species.

7.2. A Wider Census of Oxygen- and Nitrogen-Bearing Species in Star-Forming Environments

Similar comparisons can also be made for a wider set of sources of different types for which smaller inventories are present in the literature. **Figure 10** shows the abundances of the common O-bearing species (relative to CH_3OH; **Figure 10*a***) and N-bearing species (relative to HNCO; **Figure 10*b***) toward a range of sources. Tentative correlations are also seen here with abundances in agreement for the O-bearing species in most cases within a factor of about 3–5. A few outliers are seen, but no source or species systematically stands out. For the N-bearing species slightly more scatter is seen and there is no clear sign of an overall correlation compared to Sgr B2(N2). The exception to this is the ratio between NH_2CHO and HNCO, which shows a relatively constant abundance of HNCO of about 20% compared to NH_2CHO, except for Sgr B2(N2), where NH_2CHO is close to a factor of 2 more abundant than HNCO. The former value is in agreement with empirical correlations between the two species previously reported (e.g., Bisschop et al. 2007, Mendoza et al. 2014, López-Sepulcre et al. 2015). This correlation has previously been taken as evidence for the formation of NH_2CHO through the addition of H atoms to solid-phase HNCO. However, experimental evidence suggests that at least the final step in this process does not proceed with any efficiency, instead reforming HNCO (Noble et al. 2015), although other work (Haupa et al. 2019) indicates that interconversion of HNCO and NH_2CHO through the addition of H is indeed possible. A direct chemical relationship, via ice chemistry, between these two molecules therefore remains somewhat uncertain, although this does not rule out that similar chemical conditions would promote independent production of both. For example, Ligterink et al. (2018b) suggest that both molecules could form contemporaneously in the ices through radical addition.

Furthermore, some astrochemical models suggest that much of the observable gas-phase HNCO could be a product of the destruction of larger molecules, such as urea, NH_2CONH_2, through ion-molecule chemistry (Garrod et al. 2008, Tideswell et al. 2010). In this scenario, any HNCO released directly from the grains is destroyed in the gas phase much earlier on, at lower temperatures. If NH_2CONH_2 itself, a known interstellar molecule (Belloche et al. 2019), is predominantly a product of NH_2CHO, then a case for a direct chemical link between HNCO and NH_2CHO may be made. However, HNCO and NH_2CHO may simply be good independent indicators of the overall C, N, and O abundances available to the chemistry. Indeed, models by Quénard et al. (2018) indicate that these two molecules are linked through their similar response to temperature, not a direct chemical link. Correlations between chemically related molecules,

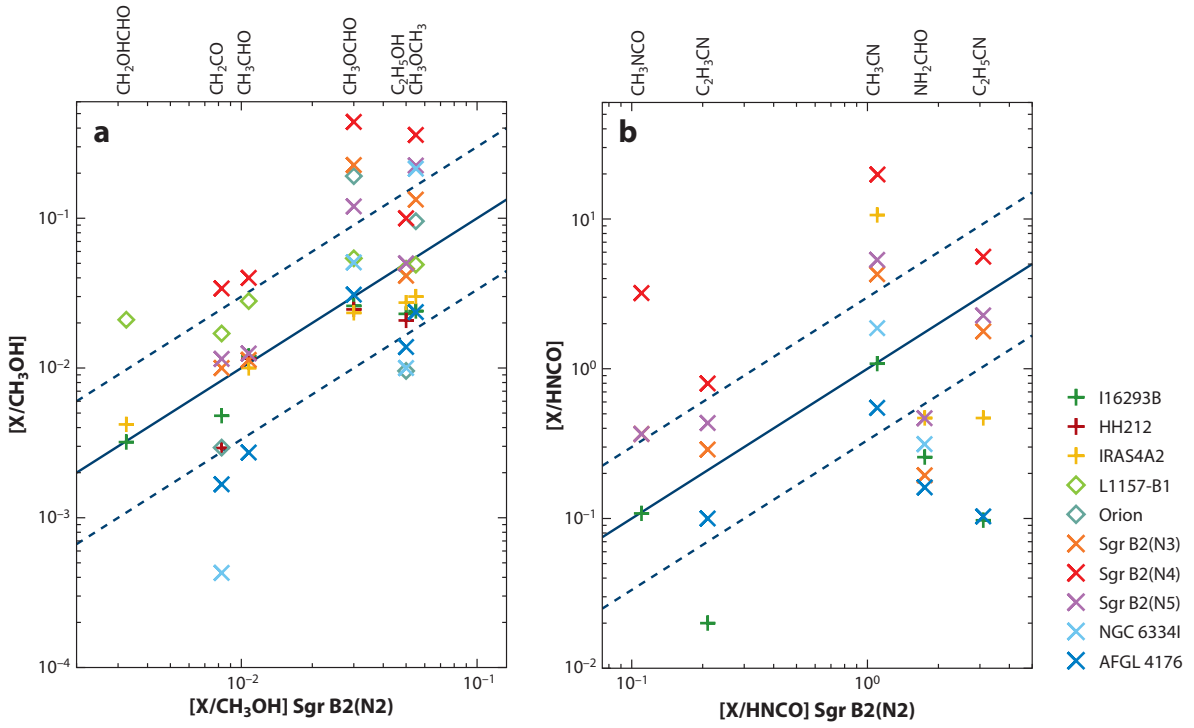

Figure 10

Comparison between the abundances of (*a*) O- and (*b*) N-bearing species toward Sgr B2(N2) (data from Müller et al. 2016a; Belloche et al. 2016, 2017; Bonfand et al. 2019; and A. Belloche, private communication) on the *x* axis and a range of sources in the literature on the *y* axis (see *legend* on the *right-hand side*): the low-mass protostellar hot corinos IRAS 16293B (Jørgensen et al. 2018, Calcutt et al. 2018b) and NGC 1333-IRAS 4A2 (López-Sepulcre et al. 2017); the possible disk atmosphere toward the low-mass protostar HH212 (Lee et al. 2019a); the shocked region B1 in the L1157 outflow; the other hot cores in Sgr B2(N), N3, N4, and N5 (Bonfand et al. 2019, and private communication); the high-mass star-forming region NGC 6334I (Zernickel et al. 2012); the Orion compact ridge (Crockett et al. 2014); and the high-mass protostar AFGL 4176 (Bøgelund et al. 2019a). The low- and high-mass sources are shown with plus signs and crosses, respectively, and the two shocks (Orion and L1157-B1) with diamonds. The abundances of the O-bearing species are measured as their column densities relative to those of CH_3OH, whereas the N-bearing species are measured relative to HNCO. The three diagonal lines in each panel indicate equal abundances (*solid*) and abundances factors of 3 above or below those in Sgr B2(N2) (*dashed*).

therefore, should not necessarily be taken to indicate a causal relationship in their interstellar production.

Clearly much work needs to be done to confirm the trends outlined above, in particular, the relatively small scatter in abundances for many COMs in Sgr B2(N2) versus IRAS 16293B, as well as the overall agreements across different types of sources. If confirmed, this trend could have important implications, i.e., that the conditions where the complex organics form are relatively homogeneous. A speculation could be that this reflects that many of the complex species form in the colder environments with the subsequent evolution (e.g., heating of gas and dust in low- versus high-mass star-forming regions or in shocks) playing a smaller role. In that case, the small scatter would provide a better defined target for models and laboratory experiments to shoot for. The possible direct detection of solid-phase COMs that are more complex than methanol in cold regions could also be highly valuable in confirming such a picture and also help in addressing the

link, if any, between the COMs observed in the gas phase toward cold prestellar cores and those in hot cores and corinos.

Furthermore, though strong similarities are seen between IRAS 16293B and Sgr B2(N2) their chemical compositions still differ from that of Comet 67P/C-G. The agreement between, e.g., the IRAS 16293B and AFGL4176 column densities (**Figure 10**) suggests that this trend may apply more generally. If confirmed through future systematic chemical inventories, this would further emphasize that chemical processing must have taken place between the protostellar and cometary stages. Accounting for this will likely be critical for addressing the relative importance of the earliest stages of star formation on any eventual chemical diversity in protoplanetary disks and (exo)planetary systems.

SUMMARY POINTS

1. Complex organic molecules (COMs) are detected in a wide range of environments ranging from cold gas in prestellar cores to the warm gas on Solar System scales close to individual protostars (Section 3).
2. The recent detections of aromatic, branched, and chiral molecules have revealed a wider range of complexity in the molecular structures available to the chemistry of star-forming regions and, by implication, to the earliest stages of protostellar and protoplanetary disk evolution (Section 3.1).
3. From a theoretical/modeling perspective, the specific formation mechanisms for individual species are still open for discussion with both grain-surface/ice and gas-phase processes providing possible formation pathways (Section 2.3).
4. Spatial differentiation between individual molecules and groups of species are seen toward some regions, which may reflect their physical structure or evolution, and/or more microphysical effects such as variations in binding energies (Section 4).
5. The influence of the detailed physical evolution of protostars on their resulting chemistry is complex, with processes such as disk formation, accretion shocks, and episodic accretion—as well as shock events such as those seen in the Orion KL region—all potentially affecting the degree of chemical processing on a source-by-source basis (Section 5). However, the importance of these effects on the end-result, e.g., in terms of the relative abundances of COMs, remains to be quantified.
6. The degree of fractionation varies between different types of regions, for example, with the enhanced deuteration of water and complex organics in low- versus high-mass star-forming regions. Systematic variations are also seen in the fractionation between groups of molecules, perhaps reflecting the conditions under which they form (Section 6).
7. Comparisons between the relative abundances of groups of molecules show promise for providing empirical insights into the origin of chemical complexity and the link to the Solar System. Specifically, excellent agreement between the abundances measured toward two significantly different regions, namely the low-mass protostar IRAS 16293B and the Galactic Center/high-mass star-forming region Sgr B2(N2), may suggest that interstellar complex chemistry is relatively robust to environmental effects (Section 7). Such correlations also set well-defined targets for future work on chemical modeling and laboratory experiments.

FUTURE ISSUES

1. The presence of COMs toward cold regions highlights the importance of understanding the composition of dust-grain ice mantles (Section 3.3). A key task for upcoming observations with the *James Webb Space Telescope* will be to reveal the composition of these ices in terms of COMs. Those observations will thereby help to define the link between the ice chemistry and the large gas-phase inventories established through observations at longer wavelengths.
2. From both physical and chemical points of views, there is significant work to do in comparing the predictions of numerical (magneto)hydrodynamical models to the molecular signatures observed toward protostars, as well as understanding, for example, the processes leading to the formation of disks and accretion through the evolution of protostars. Deeper integration of detailed chemical models with hydrodynamical simulations, to account for the chemical effects of more realistic treatments of physical evolution, would go some way to disentangling inaccuracies in the chemical treatments from the uncertainties associated purely with source structure.
3. Significant work needs to be done on expanding the large molecular inventory surveys to wider samples of sources in a systematic way. This is recognized as one of the key scientific goals of the ALMA Development Roadmap (Carpenter et al. 2018). Such upgrades will enable comparisons similar to those of **Figure 9** to many more sources in diverse environments and stages of evolution.
4. Moving forward with the characterization of the degree of molecular complexity in the gas phase of star-forming regions will require sensitive surveys that can go beyond the confusion limit reached today. Solutions may be to target lower frequencies, e.g., with ALMA and NOEMA below 80 GHz or with the Next Generation Very Large Array, or to perform high angular resolution observations to further resolve regions with narrow line widths.
5. The high angular resolution achievable with ALMA may allow astrochemical studies in the time domain such as that proposed in connection with studies of COMs in the Orion KL region and outflows (Sections 3.4 and 4.2). If indeed possible, this would be an interesting avenue to explore further.

DISCLOSURE STATEMENT

The authors are not aware of any affiliations, memberships, funding, or financial holdings that might be perceived as affecting the objectivity of this review.

ACKNOWLEDGMENTS

We are grateful to Yuri Aikawa, Geoff Blake, Paola Caselli, Eric Herbst, Niels Ligterink, Laurent Margulès, and Ewine van Dishoeck for reading and providing comments about the manuscript. Also, we thank Per Bjerkeli, Timea Csengeri, Sigurd Jensen, and Laurent Pagani for providing material used in some of the figures. J.K.J. acknowledges support by the European Research Council (ERC) under the European Union's Horizon 2020 research and innovation program through ERC Consolidator Grant "S4F" (grant agreement no. 646908). A.B. acknowledges support by the Deutsche Forschungsgemeinschaft (DFG) through the collaborative research grant

SFB 956 (project ID 184018867), subproject B3. R.T.G. acknowledges support from the NASA Astrophysics Research and Analysis program (grant NNX15AG07G), the NASA Emerging Worlds program (grant NNX17AE23G), and the NASA Astrophysics Theory Program (grant 80NSSCI8K0558).

LITERATURE CITED

Acharyya K, Herbst E. 2018. *Ap. J.* 859:51
Agúndez M, Cernicharo J, Guélin M, et al. 2008. *Astron. Astrophys.* 478:L19–22
Agúndez M, Marcelino N, Cernicharo J, Roueff E, Tafalla M. 2019. *Astron. Astrophys.* 625:A147
Aikawa Y, Wakelam V, Hersant F, Garrod RT, Herbst E. 2012. *Ap. J.* 760:40
Alexander CMO, Bowden R, Fogel ML, et al. 2012. *Science* 337:721–23
Allen DA, Burton MG. 1993. *Nature* 363:54–56
Allen M, Robinson GW. 1977. *Ap. J.* 212:396–415
Allen V, van der Tak FFS, Sánchez-Monge Á, Cesaroni R, Beltrán MT. 2017. *Astron. Astrophys.* 603:A133
Alonso ER, Kolesniková L, Tercero B, et al. 2016. *Ap. J.* 832:42
Álvarez-Barcia S, Russ P, Kästner J, Lamberts T. 2018. *MNRAS* 479:2007–15
Anderl S, Maret S, Cabrit S, et al. 2016. *Astron. Astrophys.* 591:A3
Arce HG, Santiago-García J, Jørgensen JK, Tafalla M, Bachiller R. 2008. *Ap. J. Lett.* 681:L21–24
Artur de la Villarmois E, Jørgensen JK, Kristensen LE, et al. 2019. *Astron. Astrophys.* 626:A71
Artur de la Villarmois E, Kristensen LE, Jørgensen JK, et al. 2018. *Astron. Astrophys.* 614:A26
Audard M, Ábrahám P, Dunham MM, et al. 2014. In *Protostars and Planets VI*, ed. H Beuther, RS Klessen, CP Dullemond, T Henning, pp. 387–410. Tucson: Univ. Ariz. Press
Bacmann A, Taquet V, Faure A, Kahane C, Ceccarelli C. 2012. *Astron. Astrophys.* 541:L12
Bally J, Ginsburg A, Arce H, et al. 2017. *Ap. J.* 837:60
Bally J, Zinnecker H. 2005. *Astron. J.* 129:2281–93
Balucani N, Ceccarelli C, Taquet V. 2015. *MNRAS* 449:L16–20
Barger CJ, Garrod RT. 2020. *Ap. J.* 888:38
Barone V, Latouche C, Skouteris D, et al. 2015. *MNRAS* 453:L31–35
Bell TA, Cernicharo J, Viti S, et al. 2014. *Astron. Astrophys.* 564:A114
Belloche A, Garrod RT, Müller HSP, Menten KM. 2014. *Science* 345:1584–87
Belloche A, Garrod RT, Müller HSP, et al. 2019. *Astron. Astrophys.* 628:A10
Belloche A, Meshcheryakov AA, Garrod RT, et al. 2017. *Astron. Astrophys.* 601:A49
Belloche A, Müller HSP, Garrod RT, Menten KM. 2016. *Astron. Astrophys.* 587:A91
Belloche A, Müller HSP, Menten KM, Schilke P, Comito C. 2013. *Astron. Astrophys.* 559:A47
Benedettini M, Busquet G, Lefloch B, et al. 2012. *Astron. Astrophys.* 539:L3
Bennett CJ, Chen SH, Sun BJ, Chang AHH, Kaiser RI. 2007. *Ap. J.* 660:1588–608
Bennett CJ, Hama T, Kim YS, Kawasaki M, Kaiser RI. 2011. *Ap. J.* 727:27
Bergner JB, Öberg KI, Rajappan M, Fayolle EC. 2016. *Ap. J.* 829:85
Bertin M, Romanzin C, Doronin M, et al. 2016. *Ap. J. Lett.* 817:L12
Bisschop SE, Jørgensen JK, Bourke TL, Bottinelli S, van Dishoeck EF. 2008. *Astron. Astrophys.* 488:959–68
Bisschop SE, Jørgensen JK, van Dishoeck EF, de Wachter EBM. 2007. *Astron. Astrophys.* 465:913–29
Bizzocchi L, Caselli P, Spezzano S, Leonardo E. 2014. *Astron. Astrophys.* 569:A27
Bjerkeli P, Jørgensen JK, Bergin EA, et al. 2016a. *Astron. Astrophys.* 595:A39
Bjerkeli P, Jørgensen JK, Brinch C. 2016b. *Astron. Astrophys.* 587:A145
Blake GA, Mundy LG, Carlstrom JE, et al. 1996. *Ap. J. Lett.* 472:L49
Bøgelund EG, Barr AG, Taquet V, et al. 2019a. *Astron. Astrophys.* 628:A2
Bøgelund EG, McGuire BA, Hogerheijde MR, van Dishoeck EF, Ligterink NFW. 2019b. *Astron. Astrophys.* 624:A82
Bøgelund EG, McGuire BA, Ligterink NFW, et al. 2018. *Astron. Astrophys.* 615:A88
Bonfand M, Belloche A, Garrod RT, et al. 2019. *Astron. Astrophys.* 628:A27
Bonfand M, Belloche A, Menten KM, Garrod RT, Müller HSP. 2017. *Astron. Astrophys.* 604:A60

Boogert ACA, Gerakines PA, Whittet DCB. 2015. *Annu. Rev. Astron. Astrophys.* 53:541–81
Brinch C, Jørgensen JK. 2013. *Astron. Astrophys.* 559:A82
Brouillet N, Despois D, Baudry A, et al. 2013. *Astron. Astrophys.* 550:A46
Brown PD, Charnley SB, Millar TJ. 1988. *MNRAS* 231:409–17
Burkhardt AM, Dollhopf NM, Corby JF, et al. 2016. *Ap. J.* 827:21
Burkhardt AM, Shingledecker CN, Le Gal R, et al. 2019. *Ap. J.* 881:32
Butscher T, Duvernay F, Danger G, Chiavassa T. 2016. *Astron. Astrophys.* 593:A60
Butscher T, Duvernay F, Rimola A, Segado-Centellas M, Chiavassa T. 2017. *Phys. Chem. Chem. Phys. (Inc. Faraday Trans.)* 19:2857–66
Calcutt H, Fiechter MR, Willis ER, et al. 2018a. *Astron. Astrophys.* 617:A95
Calcutt H, Jørgensen JK, Müller HSP, et al. 2018b. *Astron. Astrophys.* 616:A90
Calcutt H, Viti S, Codella C, et al. 2014. *MNRAS* 443:3157–73
Carpenter J, Iono D, Testi L, et al. 2018. *The ALMA Development Roadmap*. **https://almaobservatory.org/wp-content/uploads/2018/07/20180712-alma-development-roadmap.pdf**
Caselli P, Ceccarelli C. 2012. *Astron. Astrophys. Rev.* 20:56
Caselli P, Keto E, Bergin EA, et al. 2012. *Ap. J. Lett.* 759:L37
Caselli P, Keto E, Pagani L, et al. 2010. *Astron. Astrophys.* 521:L29
Cassen P, Moosman A. 1981. *Icarus* 48:353–76
Caswell JL. 1996. *MNRAS* 283:606–12
Ceccarelli C, Caselli P, Bockelée-Morvan D, et al. 2014. In *Protostars and Planets VI*, ed. H Beuther, RS Klessen, CP Dullemond, T Henning, pp. 859–82. Tucson: Univ. Ariz. Press
Cernicharo J, Gallego JD, López-Pérez JA, et al. 2019. *Astron. Astrophys.* 626:A34
Cernicharo J, Kisiel Z, Tercero B, et al. 2016. *Astron. Astrophys.* 587:L4
Charnley SB, Tielens AGGM, Millar TJ. 1992. *Ap. J. Lett.* 399:L71
Chuang KJ, Fedoseev G, Ioppolo S, van Dishoeck EF, Linnartz H. 2016. *MNRAS* 455:1702–12
Cleeves LI, Bergin EA, Alexander CMOD, et al. 2014. *Science* 345:1590–93
Codella C, Ceccarelli C, Bianchi E, et al. 2016. *MNRAS* 462:L75–79
Codella C, Ceccarelli C, Caselli P, et al. 2017. *Astron. Astrophys.* 605:L3
Codella C, Ceccarelli C, Lefloch B, et al. 2012. *Ap. J. Lett.* 757:L9
Codella C, Lefloch B, Ceccarelli C, et al. 2010. *Astron. Astrophys.* 518:L112
Corby J. 2016. *Astrochemistry in the Age of Broadband Radio Astronomy*. PhD Thesis, University of Virginia
Corby JF, Jones PA, Cunningham MR, et al. 2015. *MNRAS* 452:3969–93
Cordiner MA, Charnley SB, Kisiel Z, McGuire BA, Kuan YJ. 2017. *Ap. J.* 850:187
Coudert LH, Drouin BJ, Tercero B, et al. 2013. *Ap. J.* 779:119
Coudert LH, Margulès L, Vastel C, et al. 2019. *Astron. Astrophys.* 624:A70
Coutens A, Jørgensen JK, Persson MV, et al. 2014. *Ap. J. Lett.* 792:L5
Coutens A, Jørgensen JK, van der Wiel MHD, et al. 2016. *Astron. Astrophys.* 590:L6
Coutens A, Ligterink NFW, Loison JC, et al. 2019. *Astron. Astrophys.* 623:L13
Coutens A, Persson MV, Jørgensen JK, Wampfler SF, Lykke JM. 2015. *Astron. Astrophys.* 576:A5
Coutens A, Vastel C, Caux E, et al. 2012. *Astron. Astrophys.* 539:A132
Coutens A, Vastel C, Cazaux S, et al. 2013. *Astron. Astrophys.* 553:A75
Crockett NR, Bergin EA, Neill JL, et al. 2015. *Ap. J.* 806:239
Crockett NR, Bergin EA, Neill JL, et al. 2014. *Ap. J.* 787:112
Csengeri T, Belloche A, Bontemps S, et al. 2019. *Astron. Astrophys.* 632:A57
Csengeri T, Bontemps S, Wyrowski F, et al. 2018. *Astron. Astrophys.* 617:A89
Cuppen HM, Walsh C, Lamberts T, et al. 2017. *Space Sci. Rev.* 212:1–58
Dartois E, Thi W, Geballe TR, et al. 2003. *Astron. Astrophys.* 399:1009–20
Degli Esposti C, Dore L, Melosso M, et al. 2017. *Ap. J. Suppl.* 230:26
Drozdovskaya MN, van Dishoeck EF, Jørgensen JK, et al. 2018. *MNRAS* 476:4949–64
Drozdovskaya MN, van Dishoeck EF, Rubin M, Jørgensen JK, Altwegg K. 2019. *MNRAS* 490:50–79
Dulieu F, Nguyen T, Congiu E, Baouche S, Taquet V. 2019. *MNRAS* 484:L119–23
Dunham MM, Stutz AM, Allen LE, et al. 2014. In *Protostars and Planets VI*, ed. H Beuther, RS Klessen, CP Dullemond, T Henning, pp. 195–218. Tucson: Univ. Ariz. Press

Ehrenfreund P, Boogert ACA, Gerakines PA, Tielens AGGM, van Dishoeck EF. 1997. *Astron. Astrophys.* 328:649–69
El-Abd SJ, Brogan CL, Hunter TR, et al. 2019. *Ap. J.* 883:129
Enrique-Romero J, Rimola A, Ceccarelli C, Balucani N. 2016. *MNRAS* 459:L6–10
Faure A, Lique F, Remijan AJ. 2018. *J. Phys. Chem. Lett.* 9:3199–204
Faure A, Remijan AJ, Szalewicz K, Wiesenfeld L. 2014. *Ap. J.* 783:72
Favre C, Carvajal M, Field D, et al. 2014. *Ap. J. Suppl.* 215:25
Favre C, Pagani L, Goldsmith PF, et al. 2017. *Astron. Astrophys.* 604:L2
Fayolle EC, Öberg KI, Jørgensen JK, et al. 2017. *Nat. Astron.* 1:703–8
Fedoseev G, Chuang KJ, van Dishoeck EF, Ioppolo S, Linnartz H. 2016. *MNRAS* 460:4297–309
Fedoseev G, Cuppen HM, Ioppolo S, Lamberts T, Linnartz H. 2015. *MNRAS* 448:1288–97
Feng S, Beuther H, Henning T, et al. 2015. *Astron. Astrophys.* 581:A71
Fontani F, Busquet G, Palau A, et al. 2015. *Astron. Astrophys.* 575:A87
Fontani F, Codella C, Ceccarelli C, et al. 2014. *Ap. J. Lett.* 788:L43
Friedel DN, Snyder LE. 2008. *Ap. J.* 672:962–73
Frimann S, Jørgensen JK, Dunham MM, et al. 2017. *Astron. Astrophys.* 602:A120
Frimann S, Jørgensen JK, Padoan P, Haugbølle T. 2016. *Astron. Astrophys.* 587:A60
Furuya K, Aikawa Y. 2018. *Ap. J.* 857:105
Furuya K, Aikawa Y, Hincelin U, et al. 2015. *Astron. Astrophys.* 584:A124
Furuya K, Drozdovskaya MN, Visser R, et al. 2017. *Astron. Astrophys.* 599:A40
Furuya K, van Dishoeck EF, Aikawa Y. 2016. *Astron. Astrophys.* 586:A127
Gaches BAL, Offner SSR. 2018. *Ap. J.* 861:87
Garrod RT. 2008. *Astron. Astrophys.* 491:239–51
Garrod RT. 2013. *Ap. J.* 765:60
Garrod RT. 2019. *Ap. J.* 884:69
Garrod RT, Belloche A, Müller HSP, Menten KM. 2017. *Astron. Astrophys.* 601:A48
Garrod RT, Herbst E. 2006. *Astron. Astrophys.* 457:927–36
Garrod RT, Pauly T. 2011. *Ap. J.* 735:15
Garrod RT, Vasyunin AI, Semenov DA, Wiebe DS, Henning T. 2009. *Ap. J. Lett.* 700:L43–46
Garrod RT, Wakelam V, Herbst E. 2007. *Astron. Astrophys.* 467:1103–15
Garrod RT, Widicus Weaver SL, Herbst E. 2008. *Ap. J.* 682:283–302
Garrod RT, Williams DA, Hartquist TW, Rawlings JMC, Viti S. 2005. *MNRAS* 356:654–64
Gaume RA, Claussen MJ, de Pree CG, Goss WM, Mehringer DM. 1995. *Ap. J.* 449:663
Gerakines PA, Whittet DCB, Ehrenfreund P, et al. 1999. *Ap. J.* 522:357–77
Ginsburg A, Bally J, Barnes A, et al. 2018. *Ap. J.* 853:171
Goddi C, Greenhill LJ, Humphreys EML, Chandler CJ, Matthews LD. 2011. *Ap. J. Lett.* 739:L13
Goldsmith PF, Langer WD. 1999. *Ap. J.* 517:209–25
Gómez L, Rodríguez LF, Loinard L, et al. 2005. *Ap. J.* 635:1166–72
Guzmán AE, Sanhueza P, Contreras Y, et al. 2015. *Ap. J.* 815:130
Halfen DT, Apponi AJ, Woolf N, Polt R, Ziurys LM. 2006. *Ap. J.* 639:237–45
Halfen DT, Woolf NJ, Ziurys LM. 2017. *Ap. J.* 845:158
Hamberg M, Österdahl F, Thomas RD, et al. 2010. *Astron. Astrophys.* 514:A83
Harsono D, Bjerkeli P, van der Wiel MHD, et al. 2018. *Nat. Astron.* 2:646–51
Harsono D, Jørgensen JK, van Dishoeck EF, et al. 2014. *Astron. Astrophys.* 562:A77
Hasegawa TI, Herbst E. 1993. *MNRAS* 263:589
Haupa KA, Tarczay G, Lee YP. 2019. *J. Am. Chem. Soc.* 141:11614–20
Heays AN, Visser R, Gredel R, et al. 2014. *Astron. Astrophys.* 562:A61
Henderson BL, Gudipati MS. 2015. *Ap. J.* 800:66
Henkel C, Jacq T, Mauersberger R, Menten KM, Steppe H. 1987. *Astron. Astrophys.* 188:L1–4
Herbst E, van Dishoeck EF. 2009. *Annu. Rev. Astron. Astrophys.* 47:427–80
Herczeg GJ, Karska A, Bruderer S, et al. 2012. *Astron. Astrophys.* 540:A84
Hernández-Hernández V, Zapata L, Kurtz S, Garay G. 2014. *Ap. J.* 786:38

Hollis JM. 2005. In *Astrochemistry: Recent Successes and Current Challenges, Proc. IAU Symp. 231*, ed. DC Lis, GA Blake, E Herbst, pp. 227–36. Cambridge, UK: Cambridge Univ. Press
Hollis JM, Jewell PR, Lovas FJ, Remijan A. 2004a. *Ap. J. Lett.* 613:L45–48
Hollis JM, Jewell PR, Lovas FJ, Remijan A, Møllendal H. 2004b. *Ap. J. Lett.* 610:L21–24
Hollis JM, Lovas FJ, Remijan AJ, et al. 2006a. *Ap. J. Lett.* 643:L25–28
Hollis JM, Remijan AJ, Jewell PR, Lovas FJ. 2006b. *Ap. J.* 642:933–39
Hsieh TH, Murillo NM, Belloche A, et al. 2018. *Ap. J.* 854:15
Hsieh TH, Murillo NM, Belloche A, et al. 2019. *Ap. J.* 884:149
Indriolo N, Neufeld DA, Gerin M, et al. 2015. *Ap. J.* 800:40
Jacobsen SK, Jørgensen JK, Di Francesco J, et al. 2019. *Astron. Astrophys.* 629:A29
Jacq T, Baudry A, Walmsley CM, Caselli P. 1999. *Astron. Astrophys.* 347:957–66
Jacq T, Walmsley CM, Mauersberger R, et al. 1993. *Astron. Astrophys.* 271:276–81
Jensen SS, Jørgensen JK, Kristensen LE, et al. 2019. *Astron. Astrophys.* 631:A25
Jiménez-Serra I, Vasyunin AI, Caselli P, et al. 2016. *Ap. J. Lett.* 830:L6
Jin M, Garrod RT. 2020. *Ap. J. Suppl.* In press. arXiv:2006.11127
Jones PA, Burton MG, Cunningham MR, et al. 2008. *MNRAS* 386:117–37
Jones PA, Burton MG, Tothill NFH, Cunningham MR. 2011. *MNRAS* 411:2293–310
Jørgensen JK, Favre C, Bisschop SE, et al. 2012. *Ap. J. Lett.* 757:L4
Jørgensen JK, Johnstone D, van Dishoeck EF, Doty SD. 2006. *Astron. Astrophys.* 449:609–19
Jørgensen JK, Müller HSP, Calcutt H, et al. 2018. *Astron. Astrophys.* 620:A170
Jørgensen JK, van der Wiel MHD, Coutens A, et al. 2016. *Astron. Astrophys.* 595:A117
Jørgensen JK, van Dishoeck EF. 2010a. *Ap. J. Lett.* 725:L172–75
Jørgensen JK, van Dishoeck EF. 2010b. *Ap. J. Lett.* 710:L72–76
Jørgensen JK, van Dishoeck EF, Visser R, et al. 2009. *Astron. Astrophys.* 507:861–79
Jørgensen JK, Visser R, Sakai N, et al. 2013. *Ap. J. Lett.* 779:L22
Jørgensen JK, Visser R, Williams JP, Bergin EA. 2015. *Astron. Astrophys.* 579:A23
Kahane C, Ceccarelli C, Faure A, Caux E. 2013. *Ap. J. Lett.* 763:L38
Kaifu N, Morimoto M, Nagane K, et al. 1974. *Ap. J. Lett.* 191:L135–37
Kalenskii SV, Johansson LEB. 2010. *Astron. Rep.* 54:1084–104
Kalvāns J. 2018. *MNRAS* 478:2753–65
Kim HJ, Evans NJ II, Dunham MM, Lee JE, Pontoppidan KM. 2012. *Ap. J.* 758:38
Kolesniková L, Tercero B, Alonso ER, et al. 2018. *Astron. Astrophys.* 609:A24
Krim L, Jonusas M, Guillemin JC, Yáñez M, Lamsabhi AM. 2018. *Phys. Chem. Chem. Phys.* 20:19971
Le Petit F, Ruaud M, Bron E, et al. 2016. *Astron. Astrophys.* 585:A105
Lee CF, Codella C, Li ZY, Liu SY. 2019a. *Ap. J.* 876:63
Lee CF, Li ZY, Ho PTP, et al. 2017. *Ap. J.* 843:27
Lee JE. 2007. *J. Korean Astron. Soc.* 40:83–89
Lee JE, Lee S, Baek G, et al. 2019b. *Nat. Astron.* 3:314–19
Lefloch B, Ceccarelli C, Codella C, et al. 2017. *MNRAS* 469:L73–77
Li J, Shen Z, Wang J, et al. 2017. *Ap. J.* 849:115
Ligterink NFW, Calcutt H, Coutens A, et al. 2018a. *Astron. Astrophys.* 619:A28
Ligterink NFW, Coutens A, Kofman V, et al. 2017. *MNRAS* 469:2219–29
Ligterink NFW, Tenenbaum ED, van Dishoeck EF. 2015. *Astron. Astrophys.* 576:A35
Ligterink NFW, Terwisscha van Scheltinga J, Taquet V, et al. 2018b. *MNRAS* 480:3628–43
Lindberg JE, Jørgensen JK, Brinch C, et al. 2014. *Astron. Astrophys.* 566:A74
Linsky JL. 2003. *Space Sci. Rev.* 106:49–60
Lis DC, Biver N, Bockelée-Morvan D, et al. 2013. *Ap. J. Lett.* 774:L3
Liu F, Parise B, Kristensen L, et al. 2011. *Astron. Astrophys.* 527:A19
Longmore SN, Rathborne J, Bastian N, et al. 2012. *Ap. J.* 746:117
Loomis RA, Zaleski DP, Steber AL, et al. 2013. *Ap. J. Lett.* 765:L9
López-Sepulcre A, Jaber AA, Mendoza E, et al. 2015. *MNRAS* 449:2438–58
López-Sepulcre A, Sakai N, Neri R, et al. 2017. *Astron. Astrophys.* 606:A121

Lu Y, Chang Q, Aikawa Y. 2018. *Ap. J.* 869:165
Lubowich DA, Pasachoff JM, Balonek TJ, et al. 2000. *Nature* 405:1025–27
Luhman KL, Robberto M, Tan JC, et al. 2017. *Ap. J. Lett.* 838:L3
Lykke JM, Coutens A, Jørgensen JK, et al. 2017. *Astron. Astrophys.* 597:A53
Lyons JR, Young ED. 2005. *Nature* 435:317–20
Mangum JG, Shirley YL. 2015. *Publ. Astron. Soc. Pac.* 127:266
Manigand S, Calcutt H, Jørgensen JK, et al. 2019. *Astron. Astrophys.* 623:A69
Manigand S, Jørgensen JK, Calcutt H, et al. 2020. *Astron. Astrophys.* 635:A48
Margulès L, Belloche A, Müller HSP, et al. 2016. *Astron. Astrophys.* 590:A93
Margulès L, Huet TR, Demaison J, et al. 2010. *Ap. J.* 714:1120–32
Margulès L, McGuire BA, Senent ML, et al. 2017. *Astron. Astrophys.* 601:A50
Martín-Doménech R, Muñoz Caro GM, Cruz-Daz GA. 2016. *Astron. Astrophys.* 589:A107
Martin-Drumel MA, Lee KLK, Belloche A, et al. 2019. *Astron. Astrophys.* 623:A167
Mauersberger R, Henkel C, Jacq T, Walmsley CM. 1988. *Astron. Astrophys.* 194:L1–4
Mauersberger R, Henkel C, Walmsley CM, Sage LJ, Wiklind T. 1991. *Astron. Astrophys.* 247:307
McGuire BA, Burkhardt AM, Kalenskii S, et al. 2018. *Science* 359:202–5
McGuire BA, Carroll PB, Dollhopf NM, et al. 2015. *Ap. J.* 812:76
McGuire BA, Carroll PB, Loomis RA, et al. 2016. *Science* 352:1449–52
McGuire BA, Shingledecker CN, Willis ER, et al. 2017. *Ap. J. Lett.* 851:L46
Mendoza E, Lefloch B, López-Sepulcre A, et al. 2014. *MNRAS* 445:151–61
Minier V, Ellingsen SP, Norris RP, Booth RS. 2003. *Astron. Astrophys.* 403:1095–100
Molet J, Brouillet N, Nony T, et al. 2019. *Astron. Astrophys.* 626:A132
Möller T, Endres C, Schilke P. 2017. *Astron. Astrophys.* 598:A7
Motiyenko RA, Armieieva IA, Margulès L, Alekseev EA, Guillemin JC. 2019. *Astron. Astrophys.* 623:A162
Mottram JC, van Dishoeck EF, Schmalzl M, et al. 2013. *Astron. Astrophys.* 558:A126
Müller HSP, Belloche A, Xu LH, et al. 2016a. *Astron. Astrophys.* 587:A92
Müller HSP, Schlöder F, Stutzki J, Winnewisser G. 2005. *J. Mol. Struct.* 742:215–27
Müller HSP, Thorwirth S, Roth DA, Winnewisser G. 2001. *Astron. Astrophys.* 370:L49–52
Müller HSP, Walters A, Wehres N, et al. 2016b. *Astron. Astrophys.* 595:A87
Muller S, Beelen A, Black JH, et al. 2013. *Astron. Astrophys.* 551:A109
Muller S, Beelen A, Guélin M, et al. 2011. *Astron. Astrophys.* 535:A103
Muller S, Combes F, Guélin M, et al. 2014. *Astron. Astrophys.* 566:A112
Murillo NM, Lai SP, Bruderer S, Harsono D, van Dishoeck EF. 2013. *Astron. Astrophys.* 560:A103
Neill JL, Bergin EA, Lis DC, et al. 2014. *Ap. J.* 789:8
Neill JL, Crockett NR, Bergin EA, Pearson JC, Xu LH. 2013. *Ap. J.* 777:85
Neill JL, Muckle MT, Zaleski DP, et al. 2012. *Ap. J.* 755:153
Neill JL, Steber AL, Muckle MT, et al. 2011. *J. Phys. Chem. A* 115:6472–80
Neufeld DA, Hollenbach DJ. 1994. *Ap. J.* 428:170–85
Noble JA, Theule P, Congiu E, et al. 2015. *Astron. Astrophys.* 576:A91
Öberg KI. 2016. *Chem. Rev.* 116:9631–63
Öberg KI, Boamah MD, Fayolle EC, et al. 2013. *Ap. J.* 771:95
Öberg KI, Bottinelli S, Jørgensen JK, van Dishoeck EF. 2010. *Ap. J.* 716:825–34
Öberg KI, Fayolle EC, Reiter JB, Cyganowski C. 2014. *Faraday Discuss.* 168:81–101
Öberg KI, Garrod RT, van Dishoeck EF, Linnartz H. 2009. *Astron. Astrophys.* 504:891–913
Öberg KI, van der Marel N, Kristensen LE, van Dishoeck EF. 2011. *Ap. J.* 740:14
Ohishi M, Suzuki T, Hirota T, Saito M, Kaifu N. 2019. *Publ. Astron. Soc. Jpn.* 71:86
Ordu MH, Müller HSP, Walters A, et al. 2012. *Astron. Astrophys.* 541:A121
Ordu MH, Zingsheim O, Belloche A, et al. 2019. *Astron. Astrophys.* 629:A72
Ospina-Zamudio J, Favre C, Kounkel M, et al. 2019. *Astron. Astrophys.* 627:A80
Oya Y, Sakai N, López-Sepulcre A, et al. 2016. *Ap. J.* 824:88
Oya Y, Sakai N, Watanabe Y, et al. 2017. *Ap. J.* 837:174
Pagani L, Bergin E, Goldsmith PF, et al. 2019. *Astron. Astrophys.* 624:L5

Pagani L, Favre C, Goldsmith PF, et al. 2017. *Astron. Astrophys.* 604:A32
Palau A, Walsh C, Sánchez-Monge Á, et al. 2017. *MNRAS* 467:2723–52
Parise B, Castets A, Herbst E, et al. 2004. *Astron. Astrophys.* 416:159–63
Parise B, Ceccarelli C, Tielens AGGM, et al. 2002. *Astron. Astrophys.* 393:L49–53
Peng TC, Despois D, Brouillet N, et al. 2013. *Astron. Astrophys.* 554:A78
Peng TC, Despois D, Brouillet N, Parise B, Baudry A. 2012. *Astron. Astrophys.* 543:A152
Persson MV, Jørgensen JK, Müller HSP, et al. 2018. *Astron. Astrophys.* 610:A54
Persson MV, Jørgensen JK, van Dishoeck EF. 2013. *Astron. Astrophys.* 549:L3
Persson MV, Jørgensen JK, van Dishoeck EF, Harsono D. 2014. *Astron. Astrophys.* 563:A74
Pickett HM, Poynter IRL, Cohen EA, et al. 1998. *J. Quant. Spec. Radiat. Transf.* 60:883–90
Pizzarello S, Groy TL. 2011. *Geochim. Cosmochim. Acta* 75:645–56
Plambeck RL, Wright MCH, Friedel DN, et al. 2009. *Ap. J. Lett.* 704:L25–28
Polehampton ET, Baluteau JP, Ceccarelli C, Swinyard BM, Caux E. 2002. *Astron. Astrophys.* 388:L44–47
Potapov A, Jäger C, Henning T, Jonusas M, Krim L. 2017. *Ap. J.* 846:131
Poteet CA, Pontoppidan KM, Megeath ST, et al. 2013. *Ap. J.* 766:117
Prodanović T, Steigman G, Fields BD. 2010. *MNRAS* 406:1108–15
Pulliam RL, McGuire BA, Remijan AJ. 2012. *Ap. J.* 751:1
Qasim D, Fedoseev G, Chuang KJ, et al. 2019. *Astron. Astrophys.* 627:A1
Qin SL, Schilke P, Wu J, et al. 2015. *Ap. J.* 803:39
Qin SL, Wu Y, Huang M, et al. 2010. *Ap. J.* 711:399–416
Quénard D, Jiménez-Serra I, Viti S, Holdship J, Coutens A. 2018. *MNRAS* 474:2796–812
Rab C, Elbakyan V, Vorobyov E, et al. 2017. *Astron. Astrophys.* 604:A15
Remijan A, Shiao YS, Friedel DN, Meier DS, Snyder LE. 2004. *Ap. J.* 617:384–98
Remijan AJ, Hollis JM, Lovas FJ, et al. 2008. *Ap. J. Lett.* 675:L85–88
Requena-Torres MA, Martín-Pintado J, Rodríguez-Franco A, et al. 2006. *Astron. Astrophys.* 455:971–85
Rivilla VM, Beltrán MT, Cesaroni R, et al. 2017. *Astron. Astrophys.* 598:A59
Robert F, Gautier D, Dubrulle B. 2000. *Space Sci. Rev.* 92:201–24
Safron EJ, Fischer WJ, Megeath ST, et al. 2015. *Ap. J. Lett.* 800:L5
Sakai N, Oya Y, López-Sepulcre A, et al. 2016. *Ap. J. Lett.* 820:L34
Sakai N, Sakai T, Hirota T, Burton M, Yamamoto S. 2009. *Ap. J.* 697:769–86
Sakai N, Sakai T, Hirota T, et al. 2014. *Nature* 507:78–80
Sánchez-Monge Á, Schilke P, Ginsburg A, Cesaroni R, Schmiedeke A. 2018. *Astron. Astrophys.* 609:A101
Sánchez-Monge Á, Schilke P, Schmiedeke A, et al. 2017. *Astron. Astrophys.* 604:A6
Schwörer A, Sánchez-Monge Á, Schilke P, et al. 2019. *Astron. Astrophys.* 628:A6
Sewiło M, Indebetouw R, Charnley SB, et al. 2018. *Ap. J. Lett.* 853:L19
Shimonishi T, Onaka T, Kawamura A, Aikawa Y. 2016. *Ap. J.* 827:72
Shimonishi T, Watanabe Y, Nishimura Y, et al. 2018. *Ap. J.* 862:102
Shingledecker CN, Tennis J, Le Gal R, Herbst E. 2018. *Ap. J.* 861:20
Sipilä O, Caselli P, Harju J. 2015. *Astron. Astrophys.* 578:A55
Skouteris D, Balucani N, Ceccarelli C, et al. 2018. *Ap. J.* 854:135
Skouteris D, Vazart F, Ceccarelli C, et al. 2017. *MNRAS* 468:L1–5
Soma T, Sakai N, Watanabe Y, Yamamoto S. 2015. *Ap. J.* 802:74
Song L, Kästner J. 2016. *Phys. Chem. Chem. Phys. (Inc. Faraday Trans.)* 18:29278–85
Sugimura M, Yamaguchi T, Sakai T, et al. 2011. *Publ. Astron. Soc. Jpn.* 63:459–72
Suzuki T, Ohishi M, Saito M, et al. 2018. *Ap. J. Suppl.* 237:3
Taniguchi K, Saito M, Majumdar L, et al. 2018. *Ap. J.* 866:150
Taquet V, Bianchi E, Codella C, et al. 2019. *Astron. Astrophys.* 632:A19
Taquet V, Charnley SB, Sipilä O. 2014. *Ap. J.* 791:1
Taquet V, López-Sepulcre A, Ceccarelli C, et al. 2015. *Ap. J.* 804:81
Taquet V, López-Sepulcre A, Ceccarelli C, et al. 2013. *Ap. J. Lett.* 768:L29
Taquet V, Wirström ES, Charnley SB. 2016. *Ap. J.* 821:46
Taquet V, Wirström ES, Charnley SB, et al. 2017. *Astron. Astrophys.* 607:A20

Taylor KNR, Storey JWV, Sandell G, Williams PM, Zealey WJ. 1984. *Nature* 311:236–37
Tercero B, Cernicharo J, López A, et al. 2015. *Astron. Astrophys.* 582:L1
Tercero B, Cuadrado S, López A, et al. 2018. *Astron. Astrophys.* 620:L6
Thiel V, Belloche A, Menten KM, Garrod RT, Müller HSP. 2017. *Astron. Astrophys.* 605:L6
Thiel V, Belloche A, Menten KM, et al. 2019. *Astron. Astrophys.* 623:A68
Tideswell DM, Fuller GA, Millar TJ, Markwick AJ. 2010. *Astron. Astrophys.* 510:A85
Tielens AGGM. 1983. *Astron. Astrophys.* 119:177–84
Tielens AGGM. 2013. *Rev. Mod. Phys.* 85:1021–81
Tielens AGGM, Hagen W. 1982. *Astron. Astrophys.* 114:245–60
Tobin JJ, Hartmann L, Chiang HF, et al. 2012. *Nature* 492:83–85
Tychoniec Ł, Tobin JJ, Karska A, et al. 2018. *Ap. J. Suppl.* 238:19
van Dishoeck EF, Bergin EA, Lis DC, Lunine JI. 2014. In *Protostars and Planets VI*, ed. H Beuther, RS Klessen, CP Dullemond, T Henning, pp. 835–58. Tucson: Univ. Ariz. Press
van Dishoeck EF, Blake GA. 1998. *Annu. Rev. Astron. Astrophys.* 36:317–68
van Dishoeck EF, Blake GA, Jansen DJ, Groesbeck TD. 1995. *Ap. J.* 447:760
van 't Hoff MLR, Persson MV, Harsono D, et al. 2018a. *Astron. Astrophys.* 613:A29
van 't Hoff MLR, Tobin JJ, Harsono D, van Dishoeck EF. 2018b. *Astron. Astrophys.* 615:A83
van 't Hoff MLR, Tobin JJ, Trapman L, et al. 2018c. *Ap. J. Lett.* 864:L23
van 't Hoff MLR, van Dishoeck EF, Jørgensen JK, Calcutt H. 2020. *Astron. Astrophys.* 633:A7
Vastel C, Ceccarelli C, Lefloch B, Bachiller R. 2014. *Ap. J. Lett.* 795:L2
Vasyunin AI, Herbst E. 2013a. *Ap. J.* 762:86
Vasyunin AI, Herbst E. 2013b. *Ap. J.* 769:34
Vasyunina T, Vasyunin AI, Herbst E, et al. 2014. *Ap. J.* 780:85
Visser R, Bergin EA. 2012. *Ap. J. Lett.* 754:L18
Visser R, Bergin EA, Jørgensen JK. 2015. *Astron. Astrophys.* 577:A102
Visser R, Jørgensen JK, Kristensen LE, van Dishoeck EF, Bergin EA. 2013. *Ap. J.* 769:19
Visser R, van Dishoeck EF, Black JH. 2009. *Astron. Astrophys.* 503:323–43
Viti S, Collings MP, Dever JW, McCoustra MRS, Williams DA. 2004. *MNRAS* 354:1141–45
Viti S, Williams DA. 1999. *MNRAS* 305:755–62
Vuitton V, Yelle RV, Lavvas P, Klippenstein SJ. 2012. *Ap. J.* 744:11
Watson DM, Bohac CJ, Hull C, et al. 2007. *Nature* 448:1026–28
Wehres N, Hermanns M, Wilkins OH, et al. 2018b. *Astron. Astrophys.* 615:A140
Wehres N, Maßen J, Borisov K, et al. 2018a. *Phys. Chem. Chem. Phys. (Inc. Faraday Trans.)* 20:5530–44
Widicus Weaver SL. 2019. *Annu. Rev. Astron. Astrophys.* 57:79–112
Willis ER, Garrod RT, Belloche A, et al. 2020. *Astron. Astrophys.* 636:A29
Wyrowski F, Schilke P, Walmsley CM, Menten KM. 1999. *Ap. J. Lett.* 514:L43–46
Xu Y, Li JJ, Hachisuka K, et al. 2008. *Astron. Astrophys.* 485:729–34
Yamaguchi T, Takano S, Sakai N, et al. 2011. *Publ. Astron. Soc. Jpn.* 63:L37–41
Yamaguchi T, Takano S, Watanabe Y, et al. 2012. *Publ. Astron. Soc. Jpn.* 64:105
Yen HW, Koch PM, Takakuwa S, et al. 2015a. *Ap. J.* 799:193
Yen HW, Koch PM, Takakuwa S, et al. 2017. *Ap. J.* 834:178
Yen HW, Takakuwa S, Koch PM, et al. 2015b. *Ap. J.* 812:129
Zakharenko O, Lewen F, Ilyushin VV, et al. 2019. *Astron. Astrophys.* 621:A114
Zaleski DP, Seifert NA, Steber AL, et al. 2013. *Ap. J. Lett.* 765:L10
Zapata LA, Schmid-Burgk J, Ho PTP, Rodríguez LF, Menten KM. 2009. *Ap. J. Lett.* 704:L45–48
Zapata LA, Schmid-Burgk J, Menten KM. 2011. *Astron. Astrophys.* 529:A24
Zeng S, Quénard D, Jiménez-Serra I, et al. 2019. *MNRAS* 484:L43–48
Zernickel A, Schilke P, Schmiedeke A, et al. 2012. *Astron. Astrophys.* 546:A87